Modelling of Physical Petrophysical Characteristics of Potential Goru Sands in Lower Indus Basin, Pakistan.

By

Syeda Aruba Shamim (02112013008)

M.PHIL. (GEOPHYSICS)

2020-2022

DEPARTMENT OF EARTH SCIENCES
QUAID-I- AZAM UNIVERSITY

CERTIFICATE OF APPROVAL

This dissertation submitted by **SYEDA ATUBA SHAMIM** D/O **SYED KHALID SHAMIM** is accepted in its present form by the Department of Earth Sciences, Quaid-I-Azam University Islamabad as satisfying the requirement for the award of degree of **M.Phil Geophysics.**

RECOMMENDED BY

Dr. Aamir Ali
(Chairman/ Supervisor) _____

External Examiner _____

ACKNOLEDGEMENT

In the name of **Allah**, the most Beneficent, the most Merciful. All praises to **Almighty Allah**, the creator of universe. Secondly, my humblest gratitude to the **Holy Prophet Muhammad (Peace Be Upon Him)**. Without the blessing of Allah, I could not be able to complete my work as well as to be at such a place. This thesis appears in its current form due to the assistance and guidance of several people. It gives me great pleasure to express my gratitude to all those who supported me and have contributed to making this thesis possible.

I express my profound sense of reverence to **Dr. Aamir Ali Associate Professor**, who gave me the opportunity to work under his supervision on such outstanding research. His continuous support, motivation and untiring guidance have made this thesis possible. His vast knowledge, calm nature and positive criticism motivated me to push harder to get the best forms of results. I thank him for bearing my mistakes and being the "teacher" that many fails to understand the true concept of this elevated post bestowed upon them.

Also, I am immensely pleased to place on record my deep gratitude and heartfelt thanks to **Shahzaib Sheikh** and **Yawar Amin** who helped me throughout this research period, and my friends and many others without whom this course work would have been hard to be completed.

Last but not the least, I would like to acknowledge my family for their constant support, unceasing prayers, and best wishes. My parents specially to whom I thank the most who helped me most with their constant support throughout the time for the successful completion of my thesis. Those missed to be named are always close to my heart, and if not named in the acknowledgment are fully thanked.

SYEDA ARUBA SHAMIM
M.Phil. GEOPHYSICS
2020-2022

Contents

List of Figures

List of Tables

ABSTRACT

Reservoir properties are essential for quantitative and qualitative reservoir evaluation. Although the interpretation of seismic data and petrophysical analysis of well logs provides a crude analysis of the reservoir, however, the spatial distribution of reservoir characteristics is essential for economical exploitation. Furthermore, the reservoir characterization based solely on seismic and petrophysical analysis is prone to ambiguities due to numerous factors that are generally not considered. To remove the errors encountered in the well log data, rock physics modelling is applied. The objective of this study is to characterize the reservoir properties of C interval in Gambat-Latif block, Lower Indus Basin, Pakistan using rock physics modeling for well log data of Tajjal 01, 02 and subsequent estimation of spatially distributed reservoir properties over a vintage 3D seismic data. C Interval has been identified using well to seismic tie, with horizons picked on the 3D seismic data. Interpreted seismic volume shows presence of three major faults in subsurface, with faults oriented in a NW-SE direction, showing marked horizons as shallow in west and deeper in the east, with deposition of facies also showing a thickening trend towards east. Petrophysical analysis conducted in both the wells, out of which two zones of interest were marked in Tajjal-01 well showing a higher average effective porosity ranging from 10%-12%, and a low water saturation ranging from 18.3%-19.6%, whereas in well Tajjal-02, the water saturation is high i.e., 87.4%. The template used to develop the rock physics model is the unconsolidated or poorly consolidated sand (using HRS utility). Based on this model, crossplots for Vp, Vs, density, acoustic impedance, and Vp/Vs ratio have been generated to differentiate sand and shale facies within the C interval, along with identification of the fluid in the sand lithology. Results of above mentioned crossplots showed the sand facies in Tajjal-01 well with a higher deflection away from trendline, indicating gas saturated sands, while no deflection away from trendline in these crossplots of Tajjal-02 well were observed, indicating sands in Tajjl-02 being water saturated. Furthermore, the derived quantitative properties from rock physics model have been utilized to spatially estimate the acoustic impedance, identify lithology, and confirm the presence of fluid in the C sands using model-based inversion and lambda-mu-rho attribute. The picked horizons have been used to mark the spatial distribution of the quantitative reservoir properties. Model based inversion depicts low acoustic impedance anomalous zones in the sands of C interval indicating the presence of hydrocarbons. The mu-rho attribute spatially indicates low to moderate values confirming the presence of sands, while the lambda-rho attribute,

sensitive to pore fluids, confirms the presence of gas saturated sands of C interval. The results confirms that the spatially distributed properties estimated using refined well logs from rock physics model indicate the presence of hydrocarbons in the C-interval of Lower Goru Formation in the locality.

CHAPTER 01

INTRODUCTION

1.1 Introduction

Pakistan is a country with abundant mineral resources, yet many industries and day to day life runs on technology powered by hydrocarbons, which is a commodity that the country still lacks. The exploration of hydrocarbons is carried out by the industry using conventional methods; however, the exploitation of reservoirs can only be enhanced by properly characterizing the reservoirs. The estimation of key physical parameters including porosity, permeability, lower and upper reservoir limits, their lateral and vertical extent, heterogeneous nature, and the volume and type of subsurface fluids are all part of reservoir characterization (Bacon et al., 2007; Avseth et al., 2005). The data typically utilized for estimation of the reservoir properties are seismic and well log data, however Drill Stem Test (DST) and core cuttings of the wells help in constraining the data to limit uncertainties in the study. These data sets can be combined to study and estimate reservoir properties at different scales (Hearts et al., 2002; Chen and Sidney, 1997; Chopra and Marfurt, 2007; King, 1990; Lindseth, 1979). To efficiently link the data sets different interpolation or other geostatistical techniques are utilized to enhance the data to observations made in field and create a tie with the local geology (Bosch et al., 2010).

There is an understanding that even the most calibrated data set can still have erroneous recordings, hence, hindering the actual outcomes of the parameters calculated for reservoir characterization. An understanding of quality check is therefore kept on the data sets, especially the well log data set, in which certain templates can be utilized to further validate the well log data sets in the absence of core cuttings. This helps in reducing the degree of uncertainty while characterizing the reservoir rock.

Although qualitative analysis utilizes the interpretation of tracking horizons in context to the geologic structures in subsurface, following the stratigraphic normal sequence, the true goal for any geoscientist in the upstream sector lies in the mapping of zones of hydrocarbon accumulations. Seismic reflectors can be mapped spatially through travel time, but the quantitative characteristics pertaining to the reservoir are somewhat still an ambiguity. Rock physics modeling helps in setting up the relation for the reservoir parameters (porosity, water

saturation, shale volume, etc.) with the quantitative properties (acoustic impedance, shear impedance and density) (Grana and Dvorkin, 2011).

Seismic and well log data, coupled with inversion of the seismic volume set can be integrated to stem reservoir parameters (Landa et al., 2000; Simm & Bacon, 2014). The refined logs from the rock physics models can further be utilized in seismic inversion techniques to retrieve acoustic impedance from the seismic data, giving key insight to the distinctive reservoir parameters, spatial distribution of the deposition, and local petrophysical properties (Bosch et al., 2009; Angeleri and Capri, 1982; Walls et al., 2004; Yao and Gan, 2000; Grana and Dvorkin, 2011). An important aspect of seismic inversion is its ability to enhance the vertical resolution of the data (Delaplanche et al., 1982), therefore improving our interpretation, because layer-oriented impedance displays are more helpful in constraining the reservoir models (Ashcroft, 2011). The data set used in this study is a post-stack seismic 3D data and well log data of Tajjal-01, 02. The inversion techniques applied to the data set includes model-based inversion (for acoustic and shear impedance) and lamda rho-miu rho (LMR) attribute, each working on a different set of algorithms (Veeken 2007; Silva et al., 2004; Veeken and Silva et al., 2004; Ashcroft, 2011; Veeken and Rauch-Davies, 2006; Wang, 2017).

1.2 Objectives

- Structural interpretation of the study area and demarcation of the horizon of interest using time and depth contours
- Petrophysical analysis of the Tajjal-01, Tajjal-02 and Tajjal-03 to mark the favourable zones of hydrocarbon and understanding the reservoir properties of C sands.
- Utilization of rock physics modelling to refine the well log data and subsequent segregation of sands from the mixed facies of C interval on basis of quantitative properties.
- Characterization of C sand reservoir potential using post-stack model-based inversion with the help of logs developed from the rock physics model.
- Developing lamda-rho and mu-rho attributes from the acoustic and shear impedance volumes for determining the presence of fluid and confirmation of sand lithology in the reservoir respectively.

1.3 Study Area

The area of study is in the Khairpur district of Sindh in the Lower Indus Basin of Pakistan, lying on the eastern flank of Khairpur high. Khairpur high has a high geothermal gradient suffering through many stages of subsidence. It is situated at 27° 21' N and 68° 31' E having an average altitude of 47m. The block being operated by OMV is situated almost 120km southeast of Sukkur with the size of 3D project covered of 675 square kilometres wherein 10 square kilometre was approved for the purpose of dissertation, with the study area shown below in Figure 1.1.

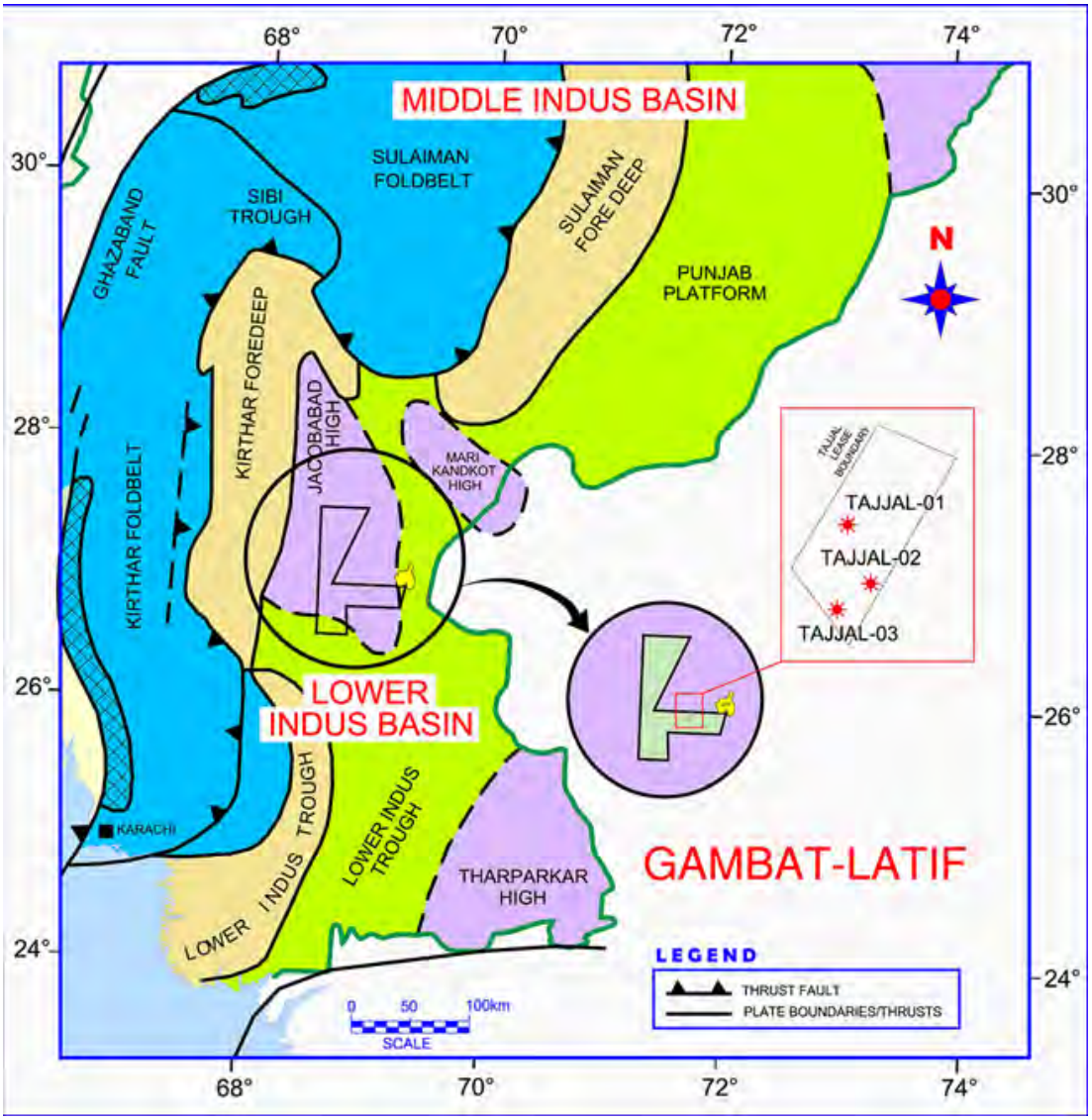

Figure 1.1 Generalized map of the study area, with block boundaries of the Gambat-Latif block highlighted in Lower Indus Basin (Kazmi and Rana, 1982).

1.4 Methodology

3D seismic data was interpreted to map the horizons and demarcate the traps that would be relevant to study. Well log data of three distinct wells Tajjal-01, Tajjal-02 and Tajjal-03 wells in combination of seismic data was utilized to tie the reflectors. The C sands mixed facies were then quantitatively analysed using rock physics modelling firstly to segregate the sand shale facies on basis of acoustic impedance, P-wave, S-wave velocity, density, and VP/VS ratio. This was achieved using different rock physics template that a sand shale facies model was established in the mixed facie interval. Finally, two different post stack inversion techniques namely model-based inversion and lamda rho miu rho (LMR) inversion were utilized to identify the spatial distribution of the C sands, and comparison of the two techniques carried out to see which was much better in characterizing the C sands and identifying their spatial distribution.

CHAPTER 02

GEOLOGY OF STUDY AREA

2.1 Introduction

In search of hydrocarbons the most essential input lies in form of the study area's tectonic settings, geology, and sequence stratigraphy. The basin's evolution can be used to fill the jigsaw puzzle of the basin's tectonic and depositional sequences (Kingston et al., 1983). Having a sound geological and structural knowledge of the study region is key for geoscientists in planning and executing geophysical studies in that region. To manage such intricate and complex plans keeping in mind the time and budget an interpreter should have a strong foundation of the geology of the region, the stratification of the lithologies, unconformities and significant structures of the study area (Kazmi & Jan, 1997). This chapter deals with a brief description of tectonic settings, structural geology, and stratigraphy of the area under study.

2.2 Structural Setting of Study Area

As discussed above the study region of the block Gambat-Latif lies in the Khairpur district of Sindh, Pakistan, which in geological terms lies in the northwester of the geologic province of the Lower Indus Basin, Pakistan. The region is characterized as an extensional regime area, and faults exist where discontinuity or contact in lithologies or bedding breaks. Normal faults are a certain characteristic of these extensional regimes, and structures associated to such faultings are usually horst and graben structures (Kadri, 1995).

The block lies to the southeast of the Kirthar fold and thrust belt, and is usually associated to as the Kirthar Foredeep, located on the continental shelf of the Indian craton. Lower Indus basin is basically a cratonic marginal basin that flanks to the northwestern side of Indian shield, thus has a high potential for many explorations plays and traps that consist of structural, stratigraphic or a combination of both. A highly mature field characterized by surrounding producing blocks can be characterized in the block owing to the mature source rock and expulsion of hydrocarbons, a good reservoir rock with a proper dip and fault bounded trap, in some area stratigraphic lenses, and lateral as well as vertical sealing rock presence to ensure integrity of the petroleum system. Mainly the reservoir rocks of the area are the sands of the Lower Goru of Cretaceous that are unconformably overlain by Deccan Basaltic flows of Paleocene, and Tertiary sedimentation (Shah et al., 1977).

2.3 Tectonics Setting

Start of the Lower Indus Basin can be characterized from the south of the Sukkur Rift Zone a combined name given to the Jacobabad-Mari Highs having an aerial extension stretching from the Balochistan basin in west to the Indian shield in the East (Raza et al., 1989).

The Main frontal thrust bounds the Kirthar fold and thrust belt in the east running along the western margin of River Indus. West of Kirthar fold and thrust belt adjoins the Chagai Magmatic Arc System and Pishin basin, with its boundary demarcated by suture zones of Bela and Muslim Bagh, having developed along strike slip components of the Chaman Fault and Ornach-Nal Fault.

Kirthar foredeep initiates from the eastern margin of the fold belt and extends eastwards to Thar Platform, which is characterized by gentle slopping monocline, extending towards the exposed Indian craton as the Nagar Parker igneous complex in the east, merging in the Kirthar trough in southwest, and bounded by Sulaiman Fold belt in the northwest (Shah,2009). The generalized tectonic map with structural settings is displayed below in Figure 2.1.

2.4 Stratigraphy of Study Area

Gambat block is covered mainly by the alluvium deposited by river Indus, with sedimentation cover being recorded throughout the geological time in the area under study. The stratigraphy of the Lower Indus basin is mostly associated to the Indian cratons rifting and drifting through the Tethyan ocean. Rifting and subsequent Kimmeridgian-Oxfordian unconformity a set development of bathyal and pelagic shales on Jurassic Chiltan limestone of the platform area can be seen with an onset of transgression with a resultant of Sembar formation with a shallow marine depositional environment is observed.

This event was subsequently followed by sea level changes and tectonics during the time which resulted into prograding siliciclastic wedges of Sembar and Goru formation s. The relative change of sea level after Sembar formation deposition, continued to change, at first causing an overall retrogradation of basin margin, through which sand bearing facies of various environments that included deltaic, shoreface and barrier islands started depositing in the form of Lower Goru of Cretaceous. However, the style changed from retrogradation to prograding, with

shale deposition sequence starting to deposit namely as Upper Goru of Early Cretaceous (Raza et al., 1989).

The important unconformities marked around study are at base of Pleocene and Plio-Miocene. Sedimentary succession comprising of Nari of Oligocene and Gaj formation of Miocene is not encountered in most of the wells, that could have been eroded or never deposited due to uplifting in Late Tertiary. The stratigraphy chart for Lower Indus basin can be seen below in Figure 2.2.

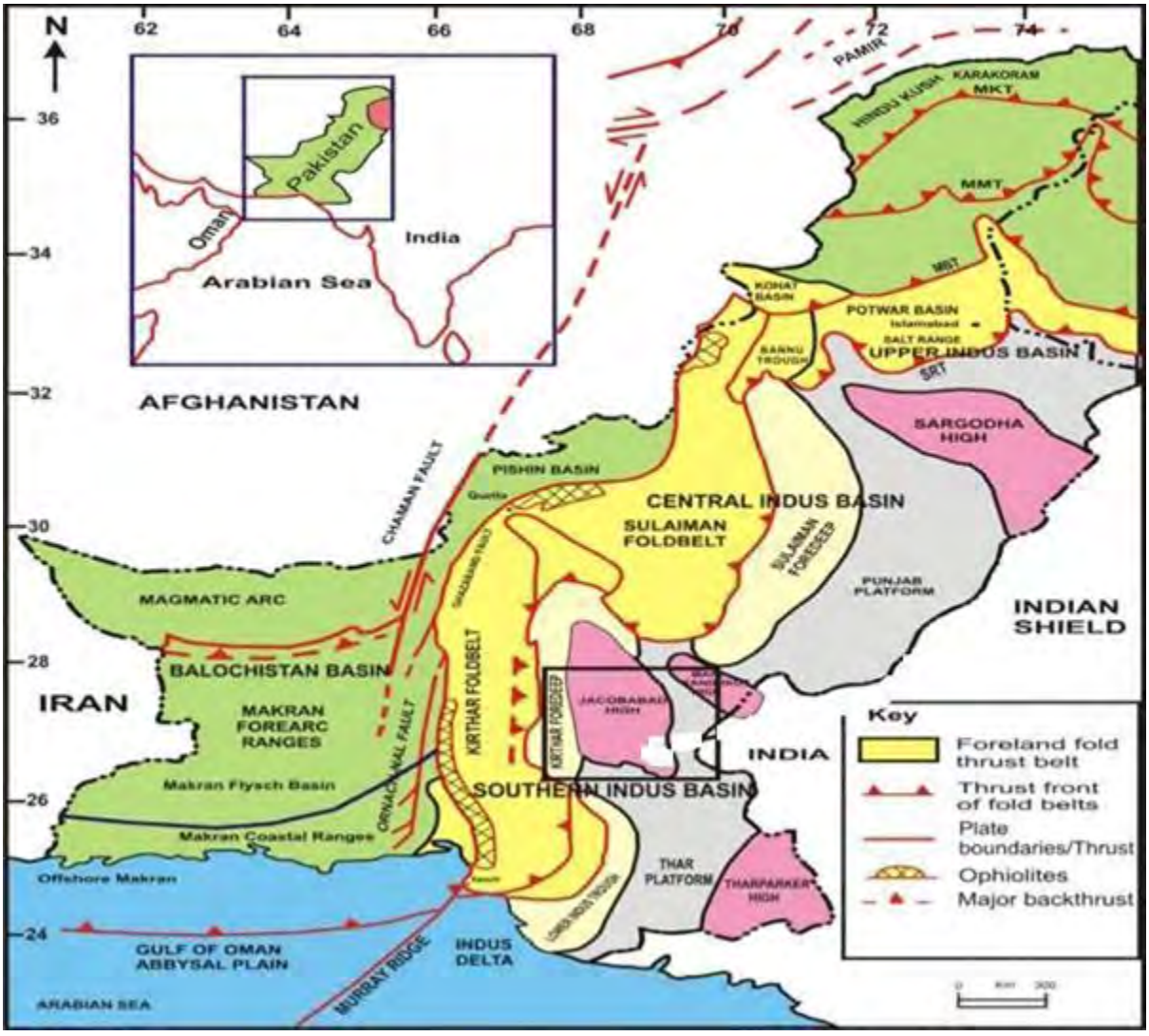

Figure 2.1 Tectonic and sedimentary basin of Pakistan (modified from Aziz & Khan, 2003), with the study area defined within the highlighted black box.

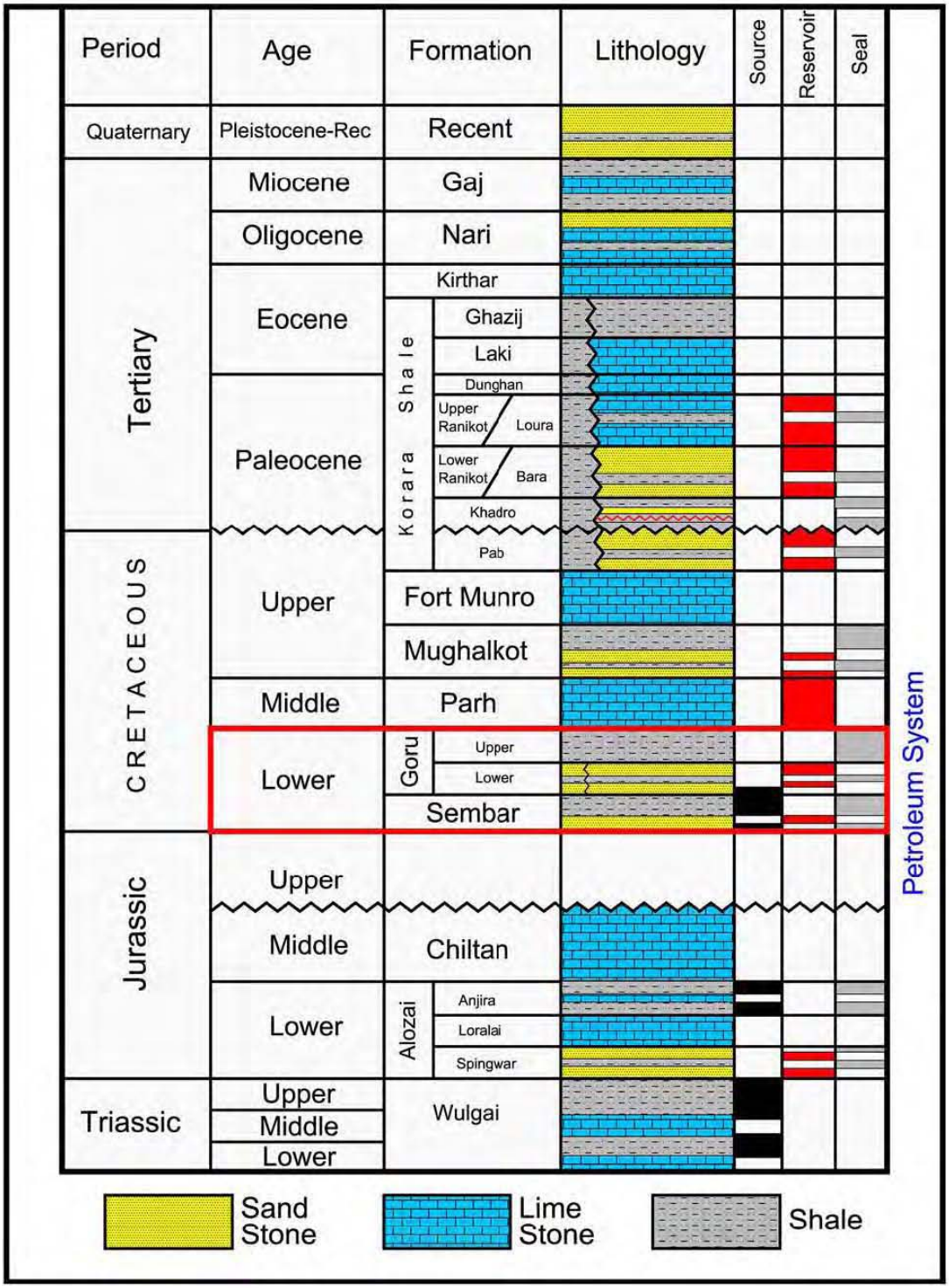

Figure 2.2 Schematic stratigraphic char of the Lower Indus Basin, with the reservoir interval under study (C sand) part of the Lower Goru formation modified from Abbasi et al., (2016).

2.5 Petroleum Play of Study Area

Before conducting any geophysical survey, identification of the petroleum play of the area is of key importance. Petroleum play is primarily based on the maturation of a source rock, expulsion, and migration of those hydrocarbons from the source rock, a reservoir rock that can store those hydrocarbons, and presence of a vertical and lateral seal rock to trap the hydrocarbons accumulated in place. A key factor that can be associated to this play is the geological age identification of the source rock maturation (Stoneley, 1995). Approximately 37% of hydrocarbon production is associated to the production from the Lower Indus Basin (Kadri, 1995).

2.5.1 Source Rock

Sembar formation mostly dominant with black silty shale, have interbedded siltstone and argillaceous limestone, of the Cretaceous age is a proven and regional source rock in the Lower and Central Indus Basin of Pakistan (Kazmi and Abbasi, 2008).

2.5.2 Reservoir Rock

The petroleum play of the Lower Indus basin has been mainly characterized to the Cretaceous age formations, with the sands of the Lower Goru formation serving as primary reservoir rock for hydrocarbon accumulation (Kadri, 1995). Lower Goru sands show an average primary porosity of around 11% in the study area (Kazmi and Rana, 1982).

2.5.3 Seal Rock

Reservoir rocks can accumulate hydrocarbons but with any other pathway they would leak out and migrate away from the reservoir rock, thus to trap and cut the access of hydrocarbons migration from reservoir rock, a presence of barrier or cap rock that acts as a seal rock, and in the lower Indus Basin, Upper Goru acts as a seal rock, but the parsequences of retrogradation and progradation during deposition of Lower Goru has deposited shale interbedding, so the mixed facies of Lower Goru formation containing shales also act as a seal rock to the sand reservoirs present in them (Kazni and Abbasi, 2008).

CHAPTER 03

3D SEISMIC DATA INTERPRETATION

3.1 Introduction

The building block to reservoir characterization stems from interpreting the seismic data set (Simm and Bacon, 2014). Seismic methods can be in simple terms be defined as the study of elastic sound waves that penetrate the earth's subsurface, using artificially sources, that work on the principles of reflection, refraction, and diffraction, and are governed by the acoustic impedance contrast of subsurface lithologies that result in the subsurface image. The resultant image is characterized as the two-way travel time image of these acoustic reflections. This information is integrated in cross-sections, which provide an image of the structure of the geological interfaces responsible for the reflection data are a bidirectional process. Subsurface modelling in which the seismic method is a key tool that can be coupled with seismic interpretation of the subsurface model are key in hydrocarbon industry. It is used to generate model and predictions about the properties and structure of subsurface. Seismic data interpretation has objective to get or extract all subsurface information from the processed seismic data. Dobrin and Savit (1988) defined interpreation as: **"The interpretation is the transformation of the seismic reflection data into structural picture by the application of correction, migration and time depth conversion."**

3.2 Base Map

The generation of a base map is the initial step of the seismic interpretation in which the 3D data set of the Gambat-Latif block containing the navigation format of the inline and crosslines were loaded along with the SEG-Y of these lines in the IHS Kingdom software, along with the wells, Tajjal-01, Tajjal-02, and Tajjal-03 that is displayed in Figure 3.1.

3.3 Seismic to Well Tie

Seismic section although does provide an image of the subsurface yet marking of reflectors particularly the reservoir and source or the seal rock remains an ambiguity, considering not knowing the depth of the horizons, which can only be obtained from the well data, hence it is principal to tie the well with seismic, to obtain pivotal information about the horizons. Tying of well and seismic does not only help in constructing the true geological sense of the study area, but also helps in constraining other parameters, such as wavelet extraction, zero phase checking etc., (Bacon et al., 2007; White, 2003; Liner, 2016; Simm and Bacon, 2014).

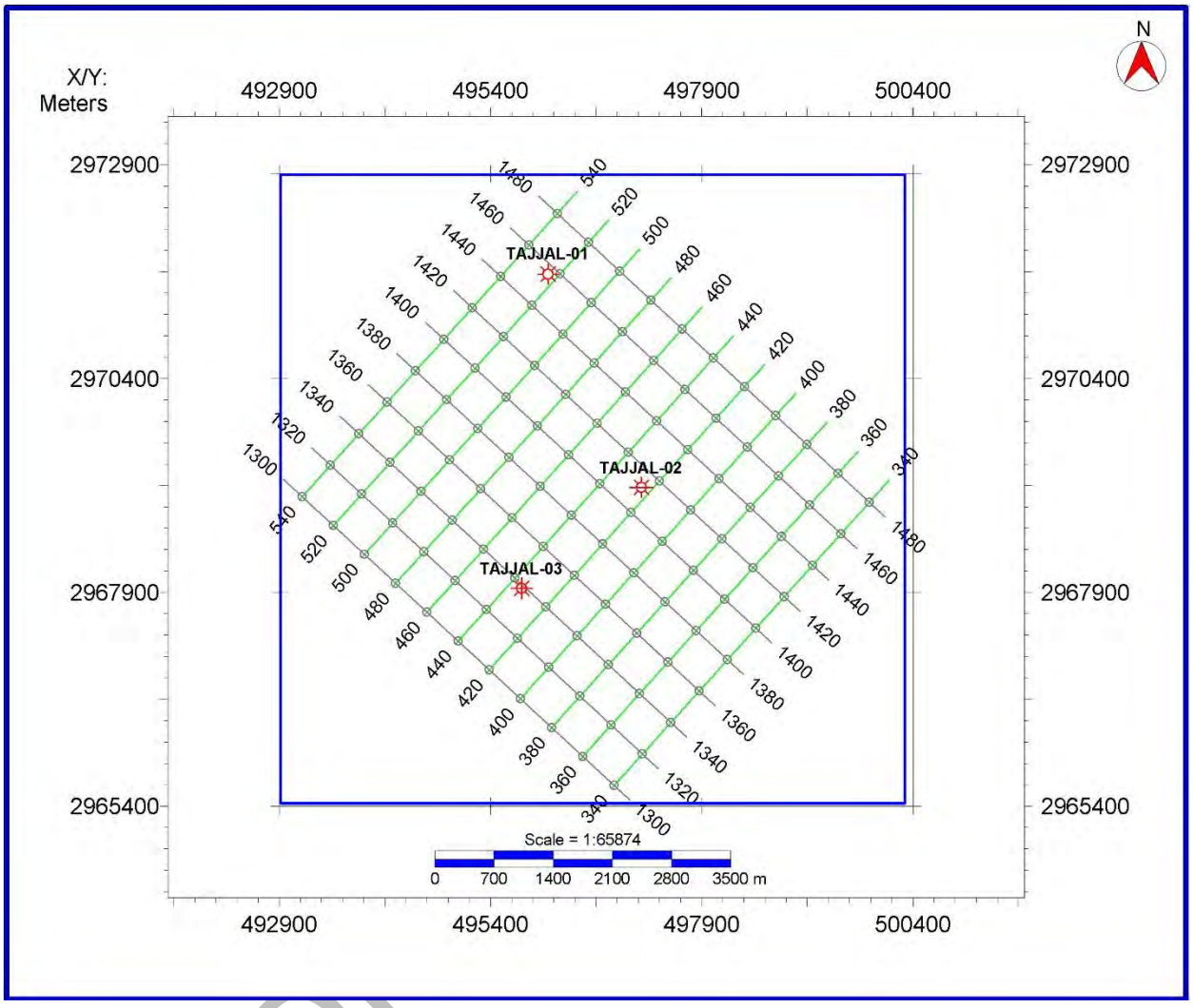

Figure 3.1 Spatial coverage of the seismic and well log data utilized in the study, with the base map constructed on IHS Kingdom software, based on Universal Transverse Mercator 42N coordinate system.

Different methods are hence taken for this approach but the most utilized is the generation of a synthetic seismogram by obtaining the reflectivity from acoustic and density logs, from well data and convolving it with the extracted seismic trace spliced along the borehole. Synthetic seismogram produced in this study of Tajjal-01 well is correlated with the seismic on inline 1454 displayed in Figure 3.2.

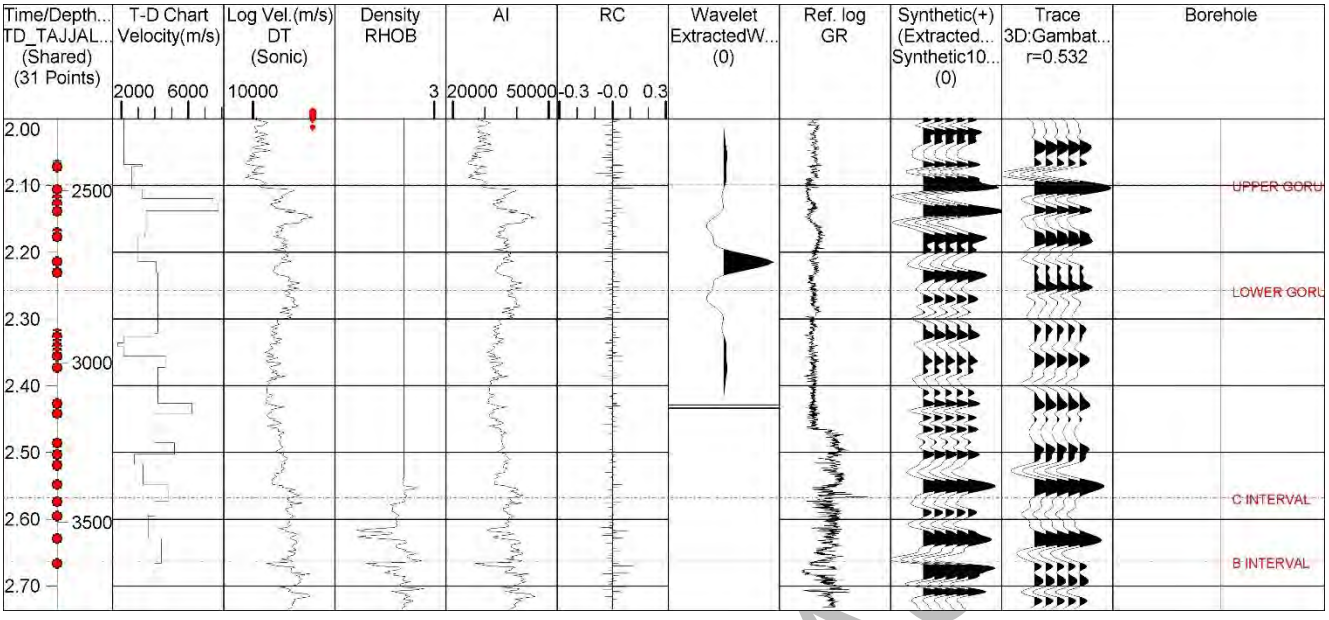

Figure 3.2 Seismic to well tie created using the sonic and density logs from Tajjal-01 las file, to generate a reflection coefficient series, that convolved with extracted wavelet and correlated with extracted trace of inline 1454 that was further used to identify horizons on the seismic section.

3.4 Faults Correlation and Fault Polygon Generation

Tectonics and geological trends are of key importance when defining the subsurface characteristics of the fault and interpreting them is crucial to identify reflector continuity and breakage. Since the study area lied in an extensional regime three major normal faults were discovered characterizing the block and were interpreted on many of the seismic inlines. These faults were then correlated and digitized to generate fault polygons, showing the direction of the faults present in the subsurface, and to characterize breakage of contours on fault polygons.

3.5 Horizon Identification

Seismic to well tie helps in correlation of the well the tops on seismic data, which in turn helps in marking the horizons on inlines and crosslines and correlating them for any mistie to be removed while horizon marking (Onajite, 2013). Prominent reflectors are marked with help of the synthetic seismogram and with help of well data from the three well so Tajjal-01, -02, and 03. With correlation from synthetic seismogram attained the horizon marking is also carried out in the IHS Kingdom software, where horizons Lower Goru, C Interval, B Interval and A interval are picked with each horizon having a different colour. A major observation recorded that the horst and graben structures and the horizons marked show and east to west trend of two-way

travel time increase, thus showing that no antithetic fault system is observed in the data set and the structure gets deeper in the west, the interpreted section can be seen in Figure 3.3.

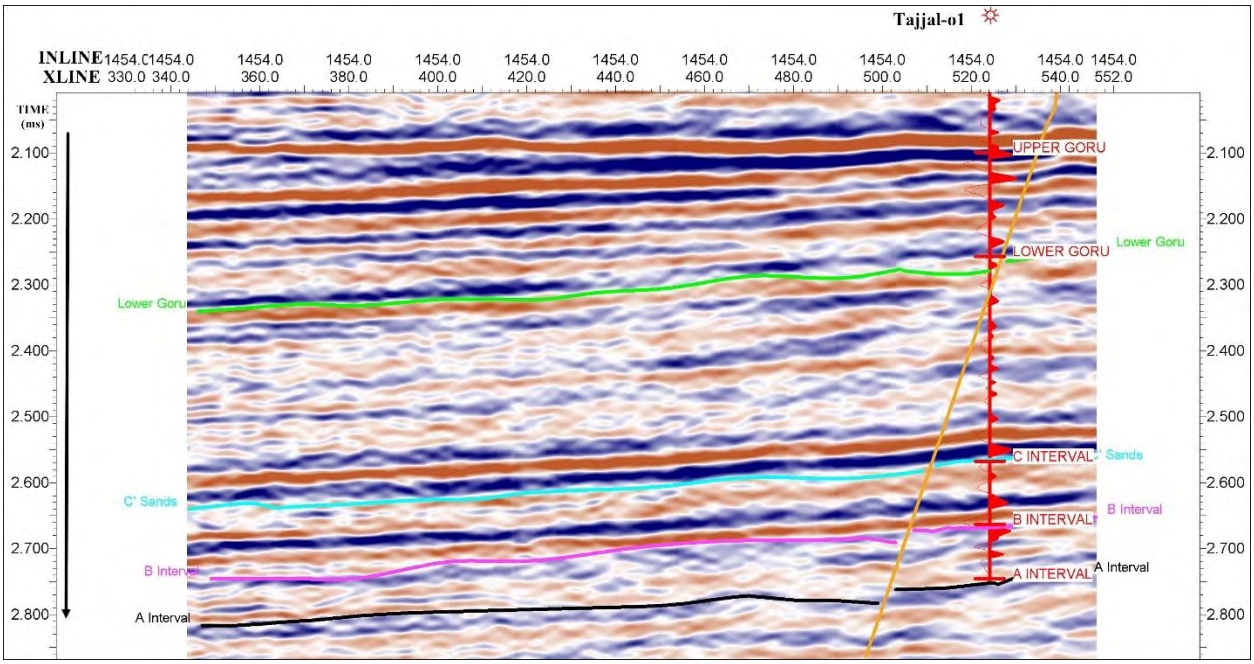

Figure 3.3 Inline 1454 with well displayed overlain by the trace obtained from seismic to well tie, marking the horizons as identified by synthetic seismogram on IHS Kingdom software.

3.6 Contour Map Preparation

Contour maps are prepared to generate contour lines that are marked by joining equal elevation, depth, time, or thickness. In oil and gas industry and typically seismic studies, time, and depth contour maps hold key importance of revealing information. These time and depth contour maps are generated in a constrained grid over the picked horizons, with different interpolation algorithms utilized to interpolate time where there is no seismic information and continuing with the general trend of the structure. Since four seismic horizons were marked that were correlated with well and synthetic seismogram a grid was constructed within the volume of the seismic cube and thus contour maps firstly of time and then later of depth were constructed.

3.7 Time Contour Map Interpretation

Time contours are prepared by joining points of equal time that have been picked through horizon picking of the reflectors, which explain about the position of horizon with respect to the travel time taken by the signal to be received on the receivers. Contours are really a basic and very significant tool to identify structures. Integrating the base map, picked horizons a time grid

or the picked horizon level is generated and the two-way travel time contour map for A interval, B interval, C interval and Lower Goru is generated which can be seen in the Figure 3.4 that shows the time variation of the A interval with a contour interval of 0.005s and a time variation of 2.815s to 2.710s. Figure 3.5 shows the B interval contour map with a contour interval of 0.004s and time variation of 2.747s to 2.625s,Figure 3.6 shows the C interval time contour map and with a contour interval of 0.004s and time variation of 2.650s to 2.526s and finally, Figure 3.7 shows the Lower Goru time contour map with a contour interval of 0.005s and time variation from 2.344s to 2.234s. The time variation that can be seen in the contour maps shows a trend of deeper structures present in the east, whereas the fault trend is in the NW-SE direction, the different coloured polygons in the grid breaking the contour values are the fault polygons which were the three major faults identified as the subsurface structure.

3.8 Depth Contour Map Interpretation

Process of preparing a depth contour map is like that of time contour maps, but the technicality that differs it from time contour maps is that it utilizes the time of the horizons that were picked and using well data information about the velocity of the lithologies, converts the time values into an approximated depth of the lithology depending on the interval velocity function chosen for accurately marking the depths. After the horizons are converted from time to depth then a depth grid is prepared of the picked horizon level of A interval, B interval, C interval and Lower Goru displayed in Figures 3.8, 3.9, 3.10 and 3.11. Figure 3.8 shows the A interval depth contour map where the contour interval was taken at 12m and the depth variation ranges from 3967m to 3713m, while Figure 3.9 shows the B interval depth contour map with contour interval of 6.25m and depth variation from 3786m to 3543m. Figure 3.10 shows the C interval depth map with a 12m contour interval and depth variation from 3594m to 3345m, and finally the Lower Goru depth map, with a 12m contour interval and depth variation from 2979m to 2754m seen in Figure 3.11. The depth and thickness of the horizons increases in the eastward direction, that can be associated the faults in the east are relatively new faults that emerged in contrast to the westward faults that are rather geologically older.

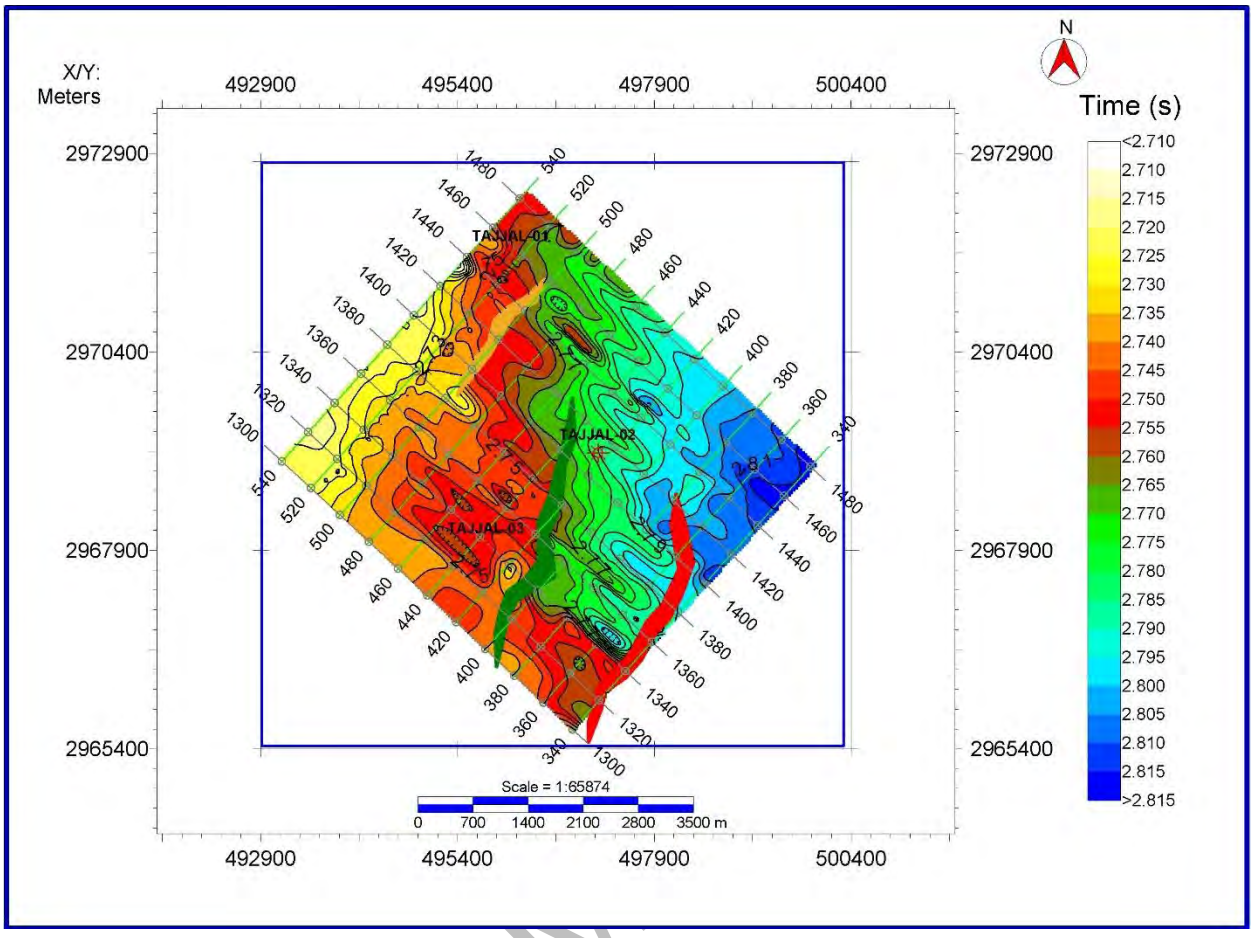

Figure 3.4 Time contour map of A interval with a contour interval of 0.005s, spatially distributed on the base map with a maximum of 2.815s and minimum of 2.71s, created on IHS Kingdom software.

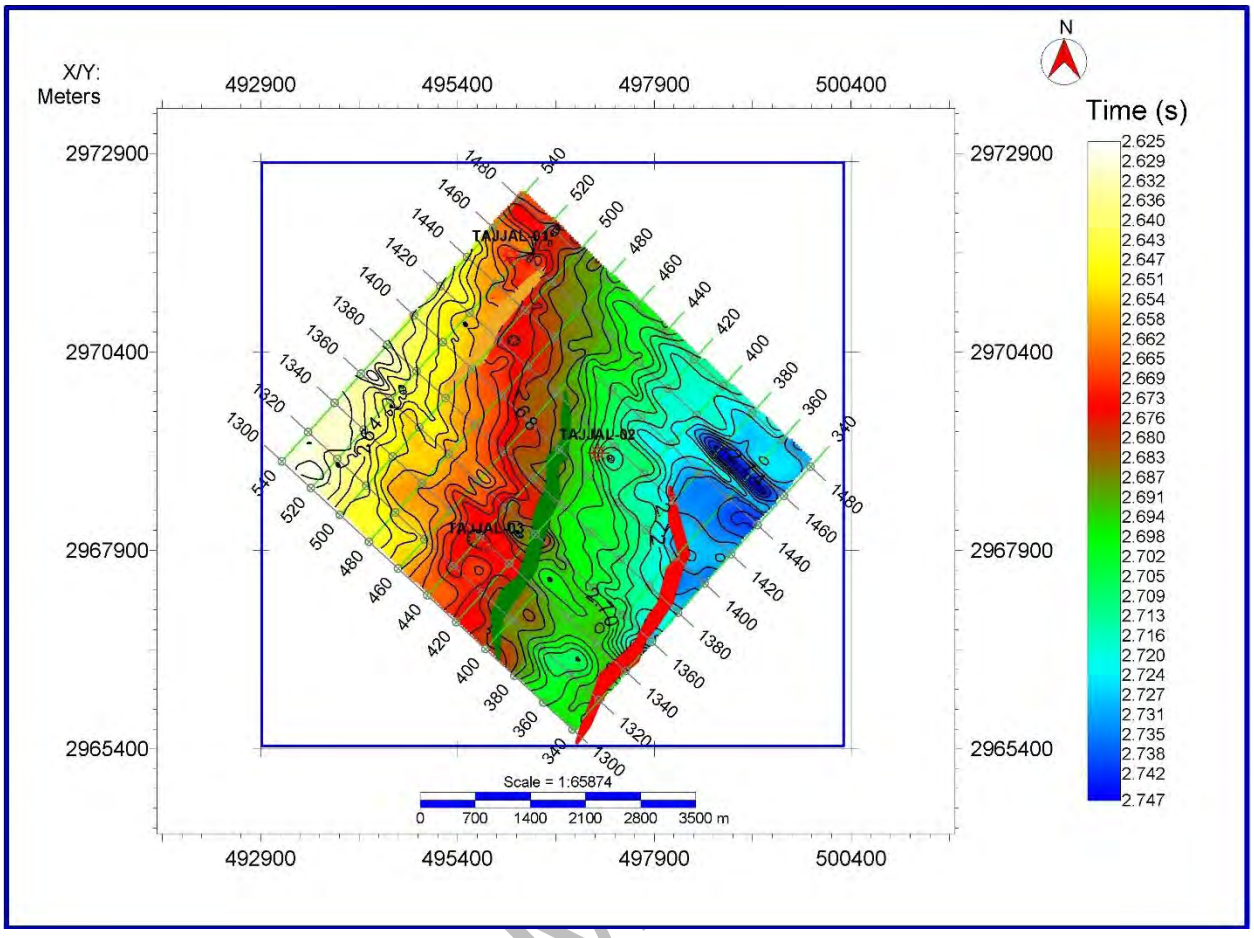

Figure 3.5 Time contour map of B interval with a contour interval of 0.004s, spatially distributed on the base map with a maximum of 2.747s and minimum of 2.625s, created on IHS Kingdom software.

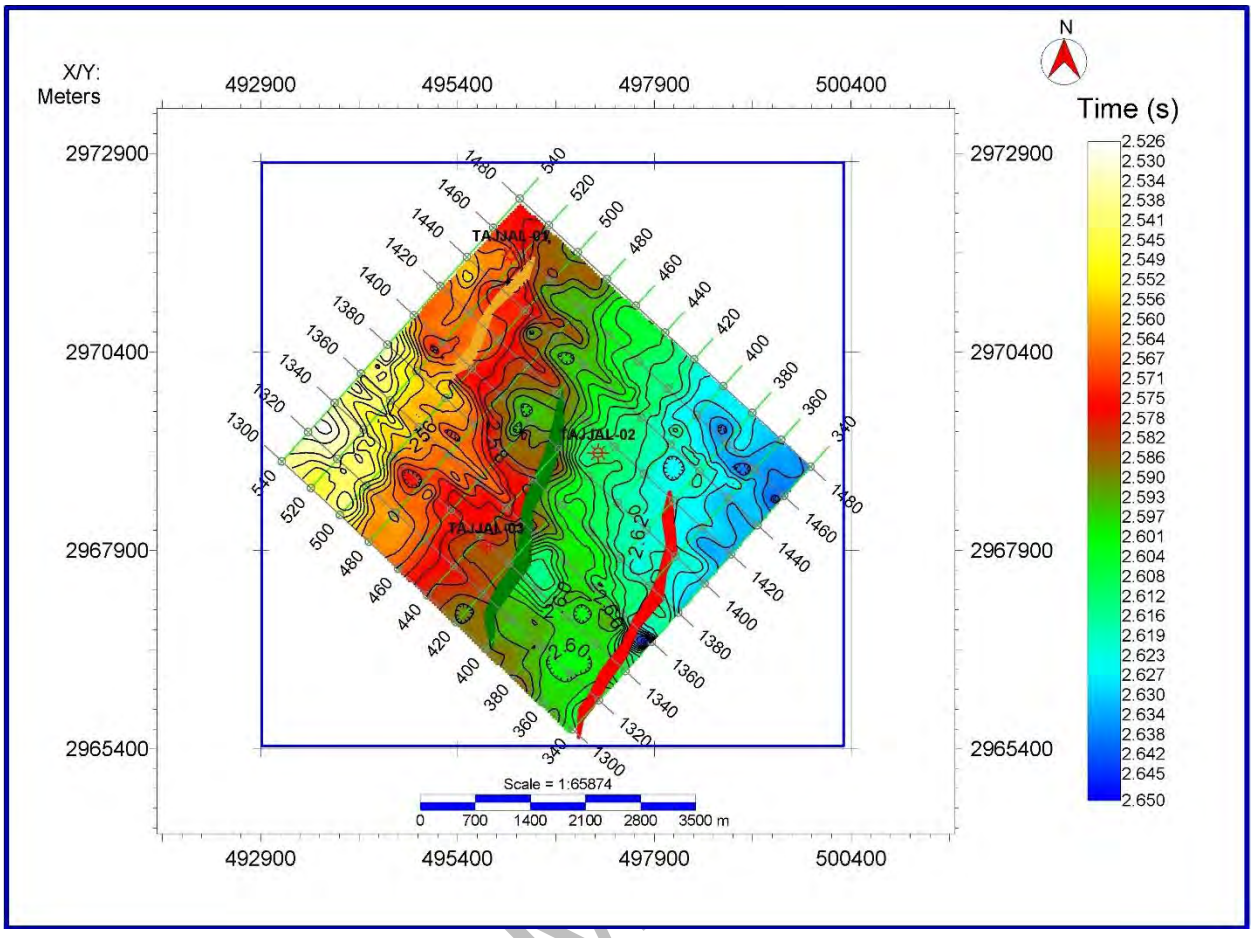

Figure 3.6 Time contour map of C interval with a contour interval of 0.004s, spatially distributed on the base map with a maximum of 2.65s and minimum of 2.526s, created on IHS Kingdom software.

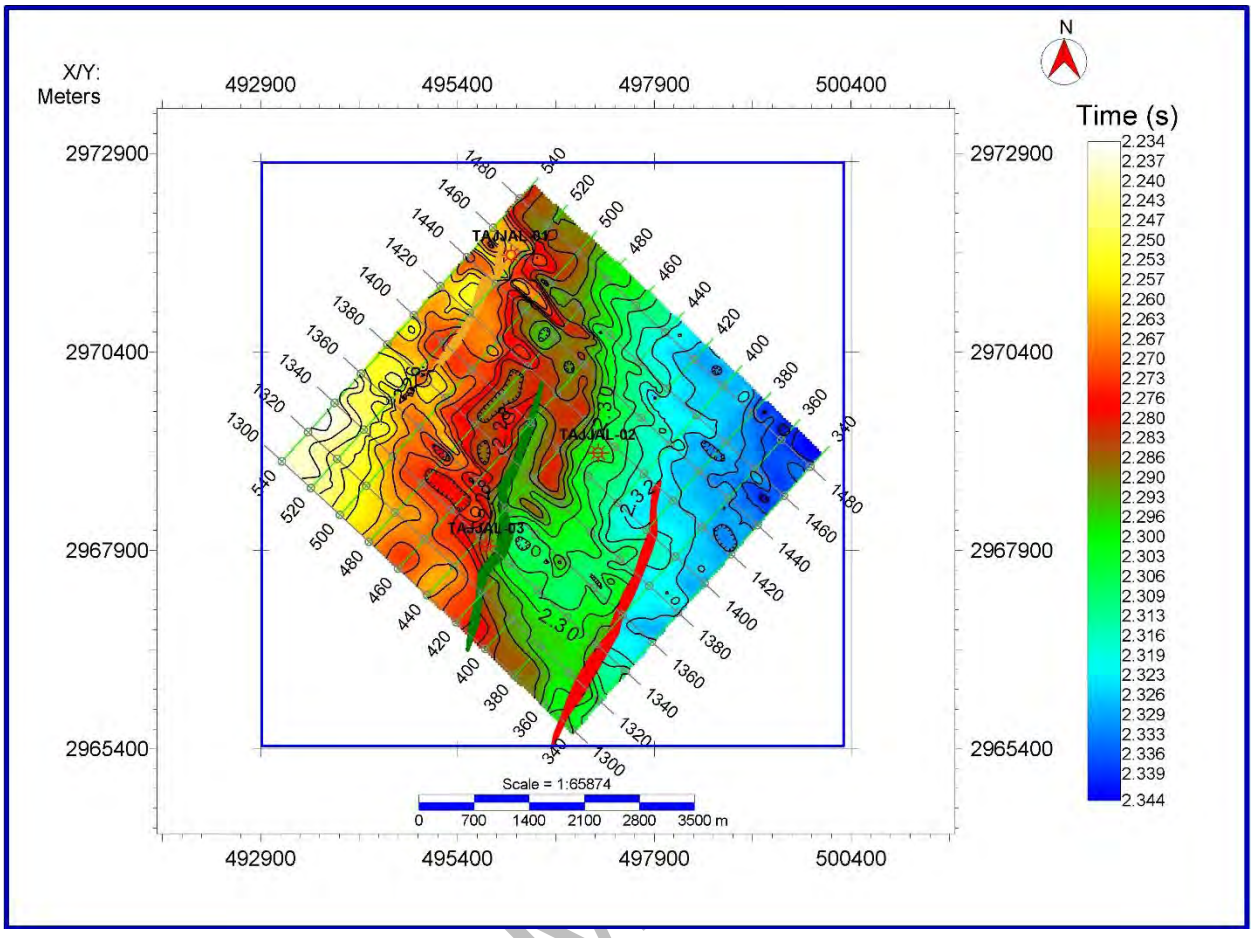

Figure 3.7 Time contour map of Lower Gorul with a contour interval of 0.005s, spatially distributed on the base map with a maximum of 2.344s and minimum of 2.234s, created on IHS Kingdom software.

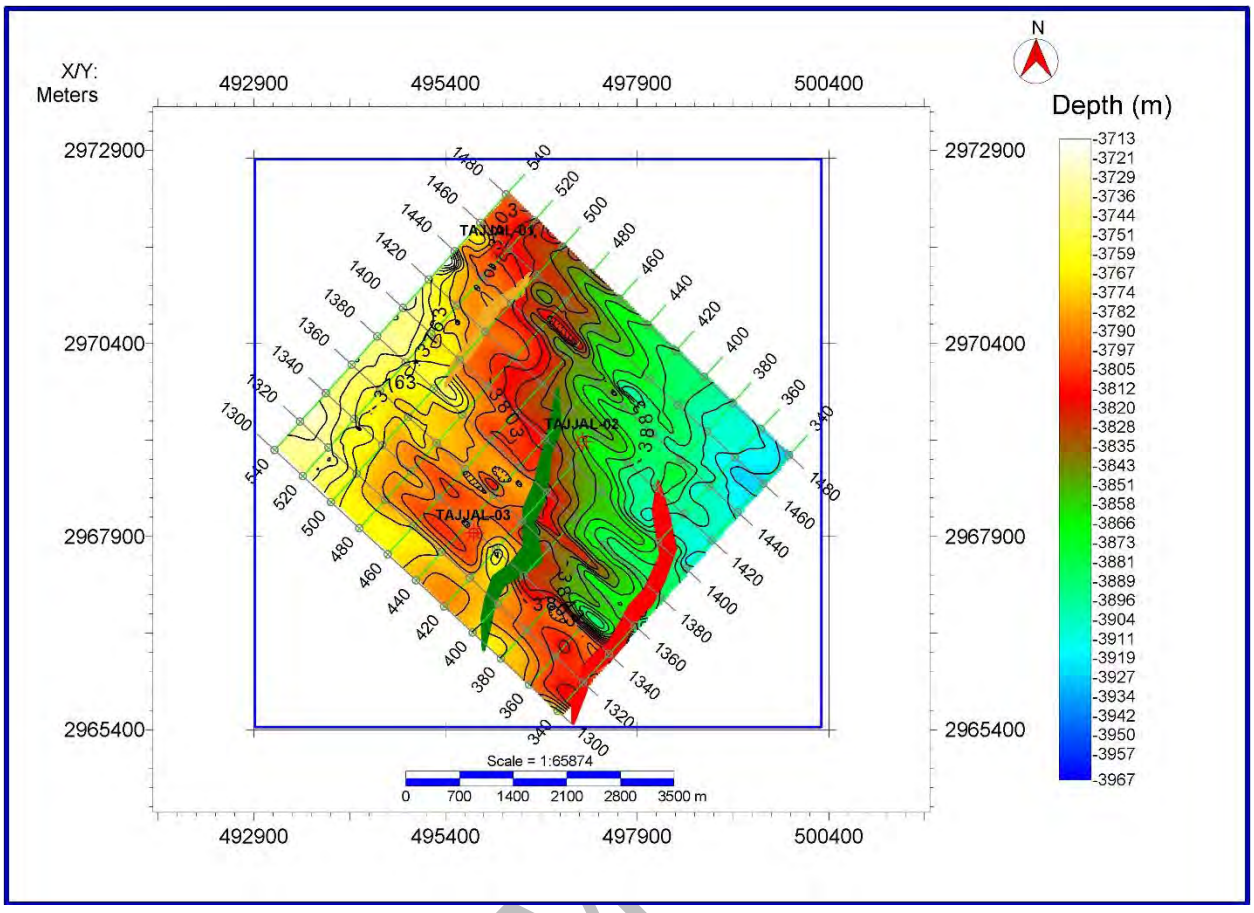

Figure 3.8 Depth contour map of A interval with a contour interval of 12m, spatially distributed on the base map with a maximum of 3967m and minimum of 3713m, created on IHS Kingdom software.

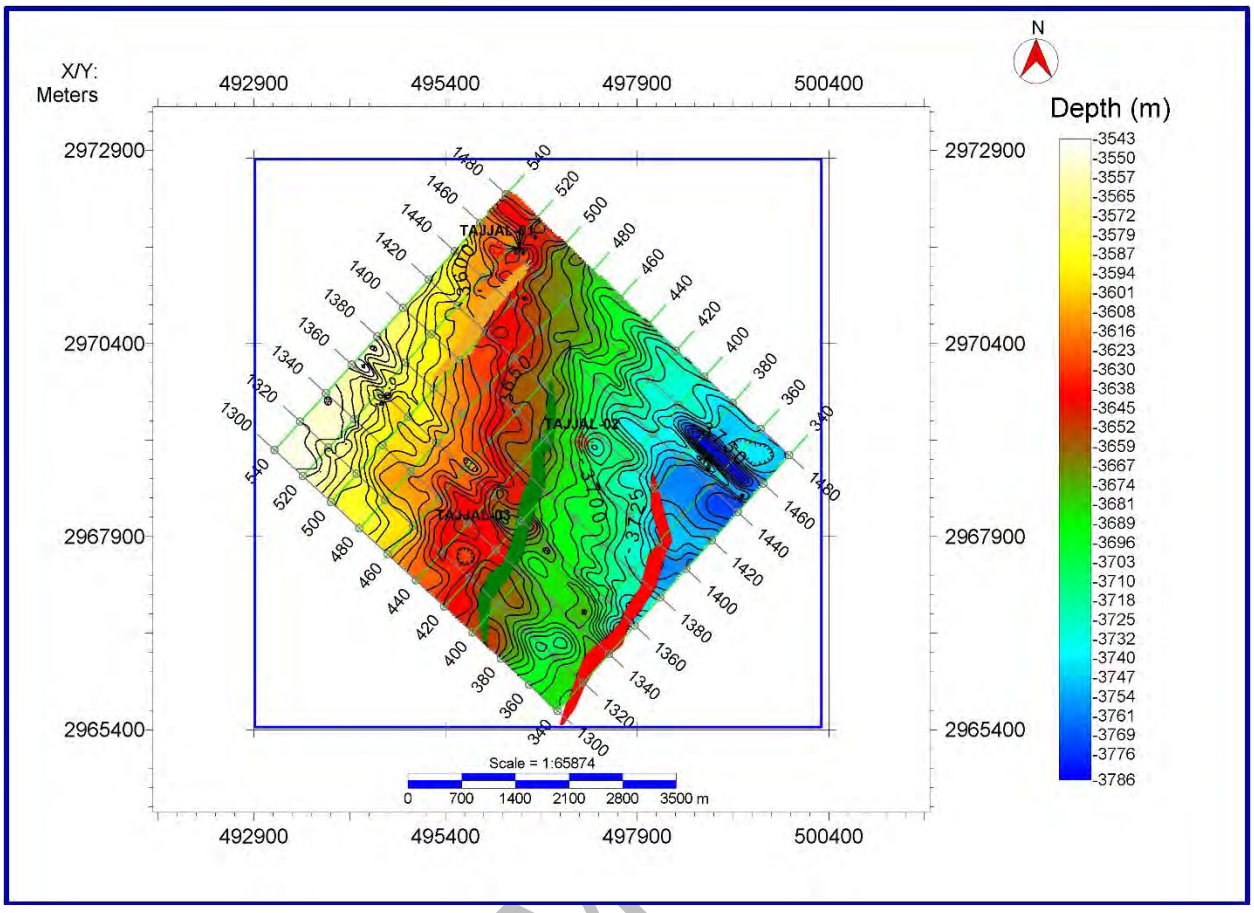

Figure 3.9 Depth contour map of B interval with a contour interval of 6.25m, spatially distributed on the base map with a maximum of 3786m and minimum of 3543m, created on IHS Kingdom software.

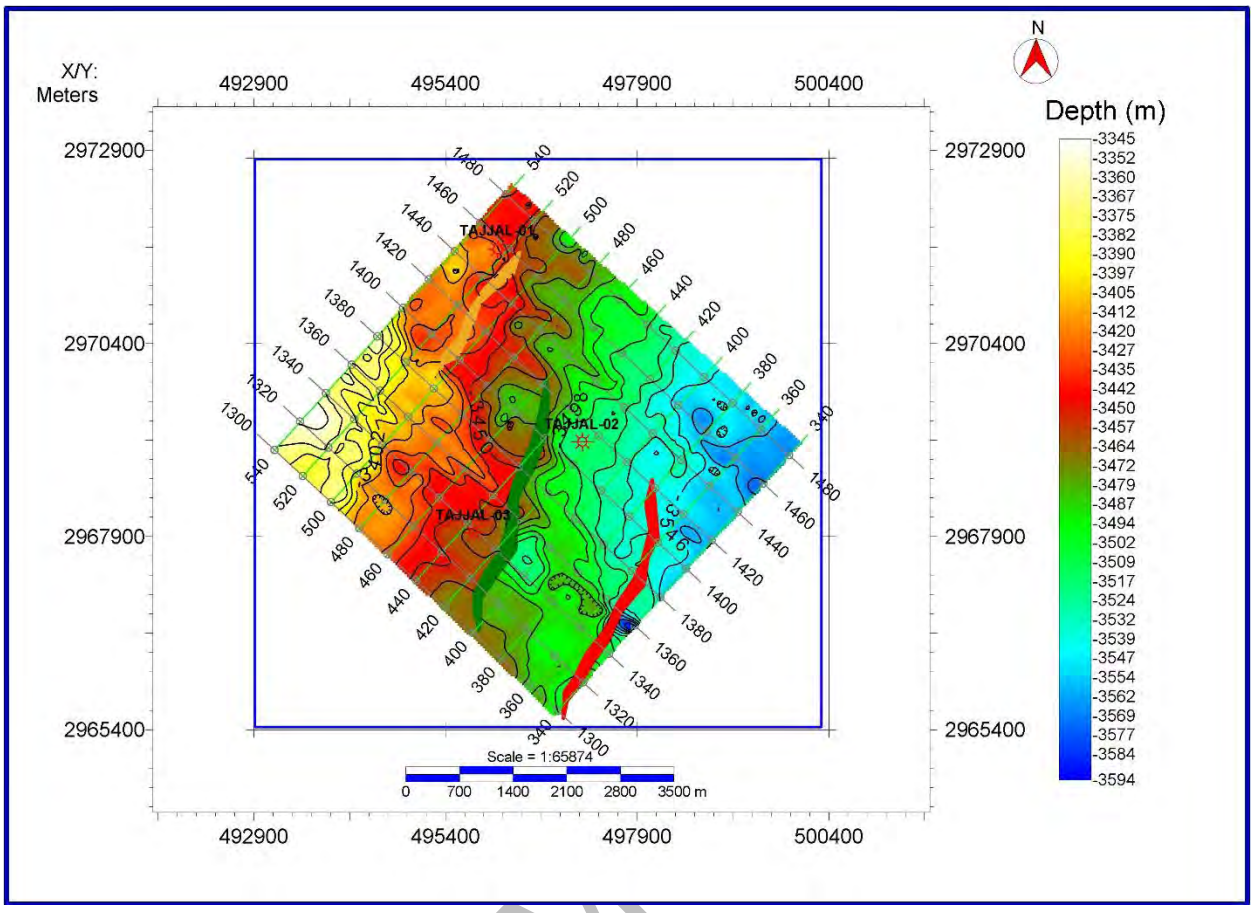

Figure 3.10 Depth contour map of C interval with a contour interval of 12m, spatially distributed on the base map with a maximum of 3594m and minimum of 3345m, created on IHS Kingdom software.

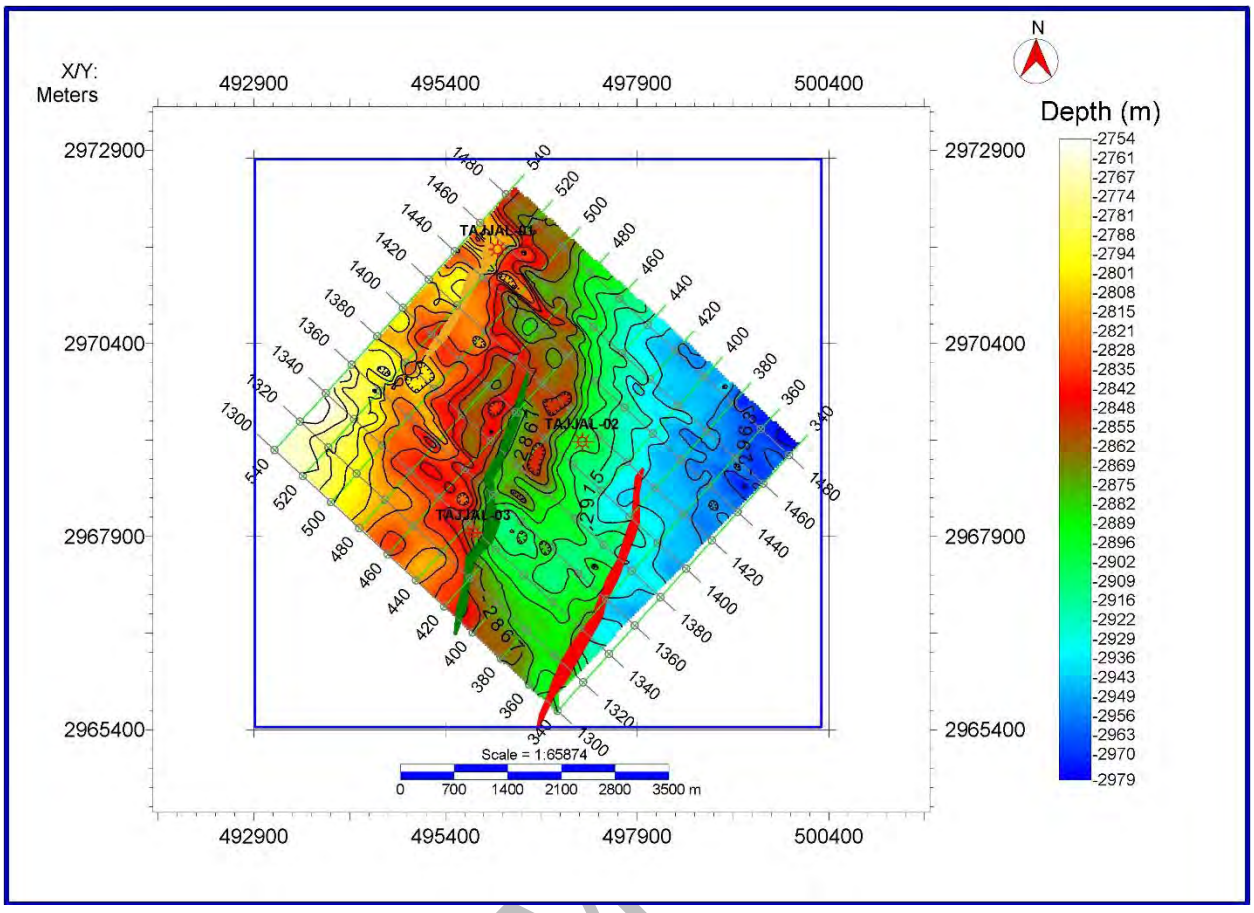

Figure 3.11 Depth contour map of Lower Goru with a contour interval of 12m, spatially distributed on the base map with a maximum of 2979m and minimum of 2754m, created on IHS Kingdom software.

CHAPTER 04

PETROPHYSICAL ANALYSIS

4.1 Introduction

Well logging is a tool to measure the subsurface properties of earth. The physical and the chemical properties of the rock explained existence and behavior of the rocks, fluids, and soils (Rider, 1996). Well logs used by the Petro physicist are caliper, resistivity, sonic (DT), gamma ray (GR), neutron (NPHI), and density (RHOB) logs etc., and all other desired information is obtained from these logs. Significance of each log cannot be ignored as they play vital role in quantifying reservoir parameters such as porosity, net pay zone, fluid content, and shale volume. Petrophysical interpretation generally has little concern with seismic, while offers detailed information about borehole measurements, ultimately contributing to reservoir characterization (Asquith et al., 2004).

4.2 Reservoir Petrophysical Properties

Petrophysicists compute reservoir petrophysical properties, which include the following.

4.2.1 Lithology

Geoscientists can use log measurement results like gamma, neutron, density, photodiodes, resistivity, as well as their combined effect to determine the lithology down hole when merged with local geology and core study.

4.2.2 Porosity (ϕ)

How much of the rock's pore (or fluid-occupied) space is occupied, this is typically determined using a device that gauges the rock's response to neutron or gamma ray bombardment. Rock porosity can also be determined and measured using NMR logs and sonic wave speed.

4.2.3 Water Saturation (Sw)

Water saturation is the percentage of pore space that is filled with water. Typically, the resistivity of rocks is measured using instruments.

4.2.4 Hydrocarbon Saturation (Sh)

The hydrocarbon saturation is a measure of how much pore space is occupied by hydrocarbons. Usually, this is calculated by deducting the water content from that one.

4.2.5 Net Pay

Rock thickness that can efficiently deliver hydrocarbon into the well bore.

4.3 Classification of Geophysical Well Logs

Well log is a profile showing different properties of formation, which is measured through wells. Every log gives some information about the subsurface. Some logs are correlated with other log to assure our prediction of lithologies. Geophysical well logs can be classified into three categories.

- Lithology logs
- Resistivity logs
- Porosity Logs

4.3.1 Lithology Logs

Lithology logs are mostly used to identify the boundaries between permeable and impervious layers, extracted information about permeable formations assist in correlation with other wells. Lithology logs are caliper (CALI), spontaneous potential (SP) and gamma ray (GR).

a) Caliper (CALI) Log

Caliper log is used to determine the diameter of the borehole. Moreover, it provides detail information about the formation's cavities portraying loose lithology along with presence of dense rocks where caving is absent. In porous layers, formation of mud cake reduces the diameter of borehole and these variations in diameter influence the logs measurements (Bjorlykke et al., 2010).

b) Gamma Ray (GR) Log

The use of gamma-ray logs allows for the measurement of a formation's natural radioactivity, also known as lithology logs. The radioactive materials have high concentration in shale while shale free sand and carbonates have low gamma-ray reading.

Volume of Shale (Vsh)

The GR log's linear method for calculating the shale volume or the gamma ray index, be calculated from equation 4.1.

$$IGR = \frac{GR_{log} - GR_{min}}{GR_{max} - GR_{min}}, \quad (4.1)$$

where, GR_{log} is the gamma ray values that are taken as input from the log, Gr_{min} is the minimum value of GR in the anomalous zone, whereas Gr_{max} is the maximum value of the GR in the ambiguous zone.

c) Spontaneous Potential (SP) Log

In the absence of any externally applied current, the borehole's natural or spontaneous voltage difference from the surface is measured by the spontaneous potential log. It is a very straightforward log that only needs a reference electrode above the surface and an electrode inside the borehole. These spontaneous potentials result from electric charge in the downhole and formation fluids having a different access to different formations, which results in a spontaneous current flow and, in turn, a spontaneous potential difference. Four main uses of this particular log is:

- Delineation of permeable formations.
- To determine the resistivity of water.
- Indicting shale within a formation.
- Correlation of wells and formation.

4.3.2 Resistivity Logs

Resistivity logs provide details about formation thickness, accurate value for the true formation resistivity and used for correlation purposes. Resistivity logs are mapped on the logarithmic scale due to get wide variation in resistivity (0.2 to 2000 ohm) with depth. Resistivity well logs are:

- Deep laterolog (LLD)
- Shallow laterolog (LLS)

a) Deep Laterolog (LLD)

Deep laterolog also termed as electrode log, mostly incorporate in measuring saltwater muds filled boreholes resistivity (Rmf). The surveying current basically controls the effective depth of this log investigation (Asquith et al., 2004).

b) Shallow Laterolog (LLS)

Shallow laterolog measures resistivity of fluids presents in invaded zone (Rt). In water beating zone, the Shallow laterolog determine a low resistivity because mud filtrate resistivity (Rmf) is almost equal to mud resistivity (Rm) (Asquith et al., 2004).

4.3.3 Porosity Logs

Porosity logs are used to measure water saturation in a formation, furthermore, it provides reliable information about lithology and porosity along with discrimination of oil and gas carrying zones.

Porosity well logs are:

- Sonic/Acoustic (DT)
- Neutron Porosity (NPHI)
- Density (RHOB)

a) Sonic /Acoustic (DT) Log

Sonic logs measure the interval transit time or DT (Δt) of the sound wave compression passing through the formation. The formation's porosity and interval transit time are related. The interval transit time is related to the porosity of the formation. The unit of measure is the microseconds per feet (Asquith et al., 2004). Porosity of the formation can be calculated by using equation 4.5.

$$\phi_s = \frac{\Delta t_{log} - \Delta t_m}{\Delta t_f - \Delta t_m}, \quad (4.5)$$

where, ϕ_s represents the calculation that is derived from the sonic log, Δt_m is the interval transient time of the matrix, Δt_{log} is the interval transit time of formation represents the transient time of the fluid (salt mud=185 and fresh mud=189). The interval transient time of the formation depends upon the matrix material, its shape, and cementation (Wyllie et al., 1956). If fluid (hydrocarbon or water) is present in the formation, transient interval time is increased, and this behavior shows increase in porosity which can be calculated by using sonic log (Asquith et al., 2004).

b) Neutron Porosity (ϕ_n) Log

Neutron porosity log is known as porosity log; basically, it is used to calculate or determine the hydrogen ion (HI) concentration in the formation (Asquith et al., 2004). The neutron log gives value of water filled porosity if the shale free formation is filled with water. In gas reservoir, porosity measured by the neutron log is low then formation true porosity as the hydrogen ions concentration is less in gas reservoir than that of oil and water (Asquith et al., 2004). It is the one limitation of neutron log that is known as the gas effect.

c) Density (RHOB) Log

This log is also known as porosity log that is used to measure electron density of the formation, (Asquith et al., 2004). Formation electron density is relative to bulks density of formation. The density logs are used with other logs and separately or different purposes (Tittman and Wahl, 1965).

Density log can be used to find out the correct porosity of the formation (Asquith and Gibson, 2004). By using equation 4.6, density porosity can be calculated as

$$\phi_d = \frac{\rho_m - \rho_b}{\rho_m - \rho_f}, \quad (4.6)$$

where, ϕ_d represents porosity derived from the density log, ρ_b represents bulk density of formation derived from the RHOB log, ρ_m represents matrix density, and ρ_f represents the density of fluid. The main purpose of present petrophysics is to obtain calculation about porosity, saturation of water and hydrocarbon.

4.4 Average Porosity (ϕ_t)

The total porosity is calculated by adding all three porosity values. Average porosity can then be calculated to get the effect of all the pores. Average porosity is measured by adding neutron porosity and density porosity values. Whereas the number of interconnected pores give effective porosity. The calculation of average porosity can be done by using equation 4.7.

$$\phi_t = (\phi N + \phi D)/2, \quad (4.7)$$

where, ϕ_t is average porosity, ϕ_D is density porosity and ϕ_N is neutron porosity.

4.5 Effective Porosity (ϕ_e)

"The proportion of the interrelated pores to the overall amount of the rock" is how it is described. The shale effect is removed from the rock unit." The zone, which is rich in shale, effective porosity would be zero. Effective porosity is used to mark the saturated zone. The effective porosity can be calculated by equation 4.8 (Asquith and Gibson, 2004).

$$\phi_e = \phi_t \times (1 - Vsh), \quad (4.8)$$

where, ϕ_e is the effective porosity which is to be calculated and ϕ_t represents the average porosity.

4.6 Water Saturation (Sw)

The proportion of a rock's pore volume that is filled with water during formation is known as water saturation. If the presence of hydrocarbons in the formation's pores is not confirmed, it is presumed that they will be filled with water. One of the fundamental purposes of well logging is to establish the saturation levels of water and hydrocarbons. To calculate saturation of water in the formation, a mathematical equation known as the Archie equation is used, which is given below as equation 4.9.

$$S_w = \sqrt[n]{\frac{F \times R_W}{R_T}}, \quad (4.9)$$

F is the formation factor where F=a/m, where Rw is the water resistivity, Rt is the true forming resistivity used in laterolog deep (LLD) applications, n is the saturation exponent, which ranges in value from 1.8 to 2.5 and therefore is taken as 2, an is consistent and its value is assumed to be 1, is the effective porosity, and m is the cementation factor, which is taken to be 2. All the other parameters to calculate R_w can be calculated from spontaneous potential logs in the following steps.

1. Pick SSP from SP log by using formula given in equation 4.10 (Rider, 1996)

   $$SSP = SP_{CLEAN} - SP_{SHALE}, \quad (4.10)$$

   SSP= Static spontaneous potential

   SP_{CLEAN}= Spontaneous potential for sand

   SP_{SHALE}= Spontaneous potential for shale

2. Determine the formation temperature FT against the depth of the reservoir formation using the equation 4.11 (Rider, 1996)

   $$FT = \left[\frac{(BHT-ST)}{TD} \times FD\right], \quad (4.11)$$

   FD= Formation depth

   BHT= Bottom hole temperature

   ST= Temperature at surface

   TD= Total depth of the borehole

3. Resistivity of the mud filtrate that is measured at surface temperature 0.17 Ωm is used to calculate the resistivity of mud filtrate at zone of interest calculated by equation 4.12.

$$R_{mf2} = \frac{(ST+6.77)\times R_{mf1}}{(FT+6.77)}\ , \qquad (4.12)$$

ST= Temperature at surface

FT= Formation Temperature

R_{mf1}= Resistivity of mud filtrate measured at surface temperature

4. The next step is to calculate the resistivity of the mud filtrate but for that if R_{mf2} is greater than 0.1 Ωm then R_{mfe} is calculated by equation 4.13

$$R_{mfeq} = 0.85 \times R_{mf2}, \qquad (4.13)$$

If R_{mf2} is less than 0.1 Ωm then we use chart SP-1 (Schlumberger Chart) given in appendix-2 to derive a value of R_{mfe} at formation temperature, as shown in the Figure 4.1. The second bar in the figure contains the R_{we} values and using the values of SSP, FT and R_{mfe}, R_{we} value is calculated which is 0.0048 Ωm.

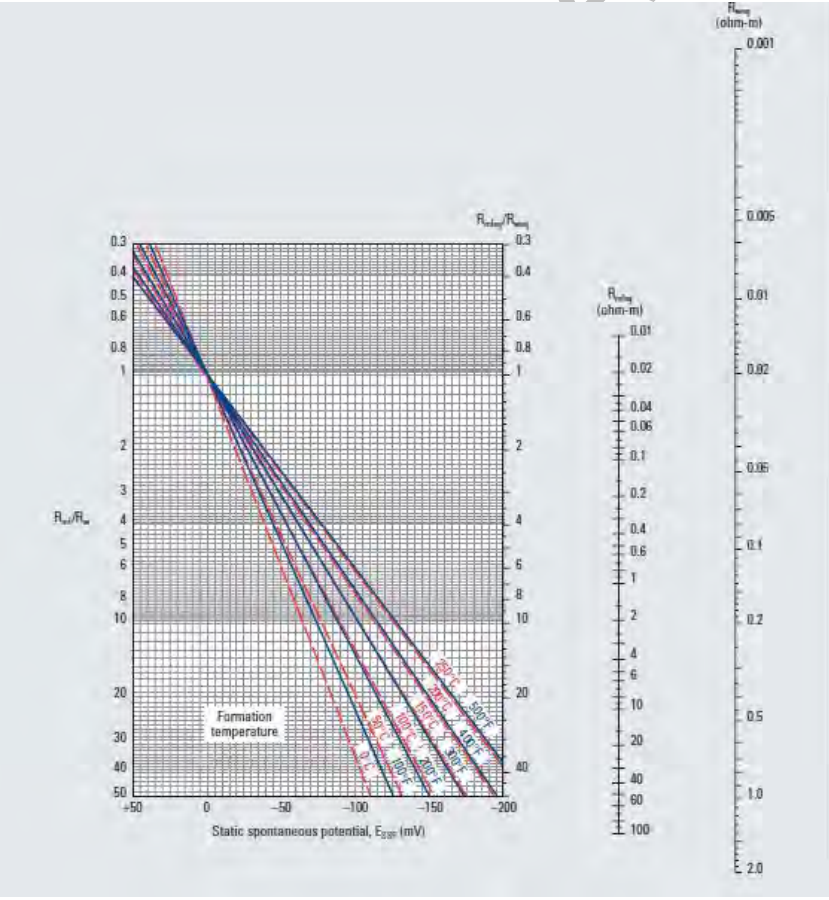

Figure 4.1 Determination of Rweq from SP-1 chart that uses the well data from header file, to find resistivity of water equivalent (Schlumberger, 1989).

5. The last step is to calculate the value of R_w after obtaining the value of R_{we} from the SP-1 chart, so we use FT and R_{we} values and use the SP-3 chart to calculate R_w, given below in Figure 4.2.

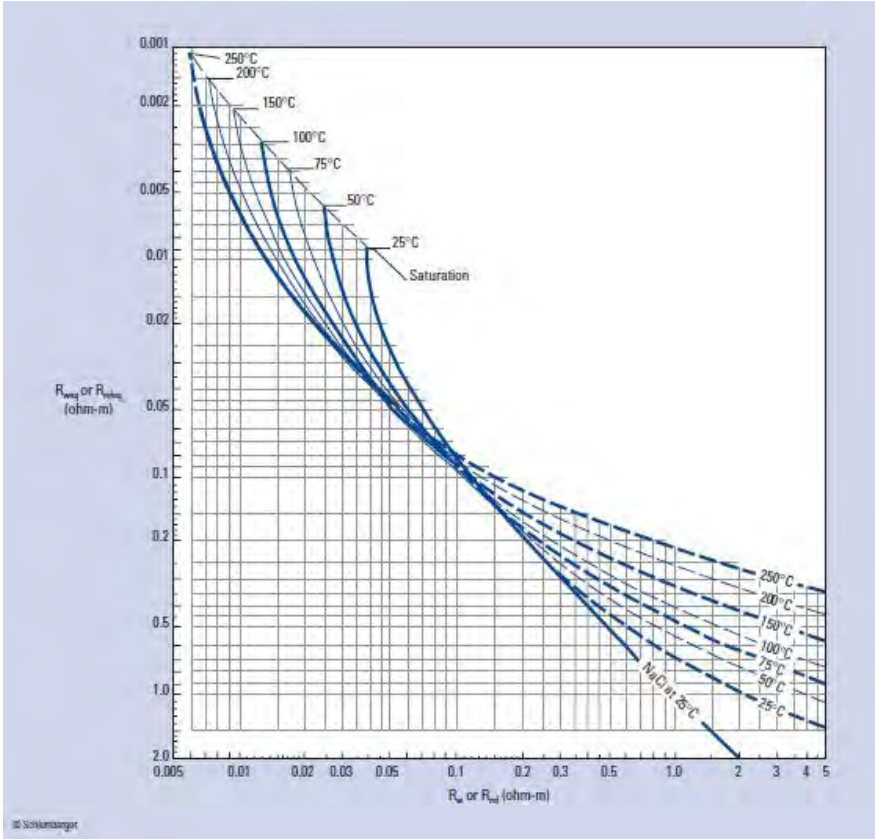

Figure 4.2 Determination of Rw from SP-3 chart after determining Rweq and using formation temperature curves can be utilized to determine where Rw for given well fits best (Schlumberger, 1989).

The resistivity of water calculated for C interval sands is 0.016 Ωm, after calculating all these parameters we use these values in Archie equation for calculating the saturation of water.

4.7 Hydrocarbon Saturation (Sh)

Hydrocarbon saturation can be defined as "the pore in the formation is filled with hydrocarbon." Equation 4.14 is used to calculate the hydrocarbon saturation.

$$Sh = 1 - Sw\,, \qquad (4.14)$$

where, Sw represents the water saturation, Sh represents the hydrocarbon saturation.

4.8 Interpretation of Well Logs

Interpreting well logs with a few indications is a very easy task, but that is if there is no inconsistency in the data set or any flaw in the borehole geometry, with issues such as borehole

breakouts, rugosity effect, or cavings that may occur in unconsolidated lithologies to cause erroneous interpretations. For this instance, the stability of caliper log is of crucial importance especially in the reservoir formation. Powerlog software was utilized to interpret the well logs of Tajjal-01 and Tajjal-02 wells, while limited data of Tajjal-03 well hindered its interpretation. Although common utilization of the GR log is to determine the reservoir as clean or dirty, but if the GR log is not present, then the use of SP log is rather a secondary piece of information that determines sands from shales. The separation of the LLD and LLS logs indicates fluid variation within the reservoir, with a higher separation indicative of gas, and smaller separation shows presence of oil respectively, with both showing higher resistivity. Porosity logs such as NPHI and RHOB also serve as clear hand indications of presence of porosity and fluid in the formation, such that both the logs decrease and since are placed in the same track and in reverse condition, with decreasing values form a crossover, that coupled with separation of LLD and LLS logs, provide first indications of presence of hydrocarbons. GR log can be further used to detect volume of shales, and a cut-off of 40% can further distinguish the sand and shale facies in the reservoir formation. Values below this cut-off indicate presence of sands and values higher than this can indicate presence of shales.

Petrophysical research on the Lower Goru formation's C-Interval on Tajjal-01 and Tajjal-02 wells at a depth of 3479m-3672m in Tajjal-01 well, and 3529m-3727m in Tajjal-02 wells. The gas producing Tajjal-01 well showed two zones of depth from 3568m to 3567m and 3585m to 3596m of potential hydrocarbon accumulation with clear indicatives and are characterized below in Table 4.1 and for Tajjal-02 in Table 4.2, whereas the abandoned well Tajjal-02 well as water saturated although showed hydrocarbon accumulation but with no crossovers forming, or high hydrocarbon resistivity, or separation between LLD and LLS logs, no potential zones were marked in Tajjal-02 well. The results of both the wells petrophysical analysis are displayed below in Figure 4.3 and 4.4.

Table 4.1 Results determined for petrophysical analysis of Tajjal-01 well with two zones of interest identified, with their calculate attributes of porosity, volume of shale, water saturation, and hydrocarbon saturation being the following.

Serial Number	**Calculation Parameters**	**Zone 1**	**Zone 2**
1	Average Volume of Shale = Vsh_{avg}	39.4%	42%
2	Average Effective Porosity in Percentage = ϕ_{eavg}	12.6%	12.1%
3	Average Water Saturation in Percentage = S_{wavg}	18.3%	19.6%
4	Average Hydrocarbon Saturation in Percentage = S_{havg}	81.7%	80.5%

Table 4.2 Petrophysical results obtained for Tajjal-02 well with no zone of interest identified, showing a higher water saturation in the well, not marking any suitable prospect and can also be concluded as well near the extent of the gas water contact.

Serial Number	**Calculation Parameters**	**C Interval**
1	Average Volume of Shale = Vsh_{avg}	43.7%
2	Average Effective Porosity in Percentage = ϕ_{eavg}	10.7%
3	Average Water Saturation in Percentage = S_{wavg}	87.4%
4	Average Hydrocarbon Saturation in Percentage = S_{havg}	12.6%

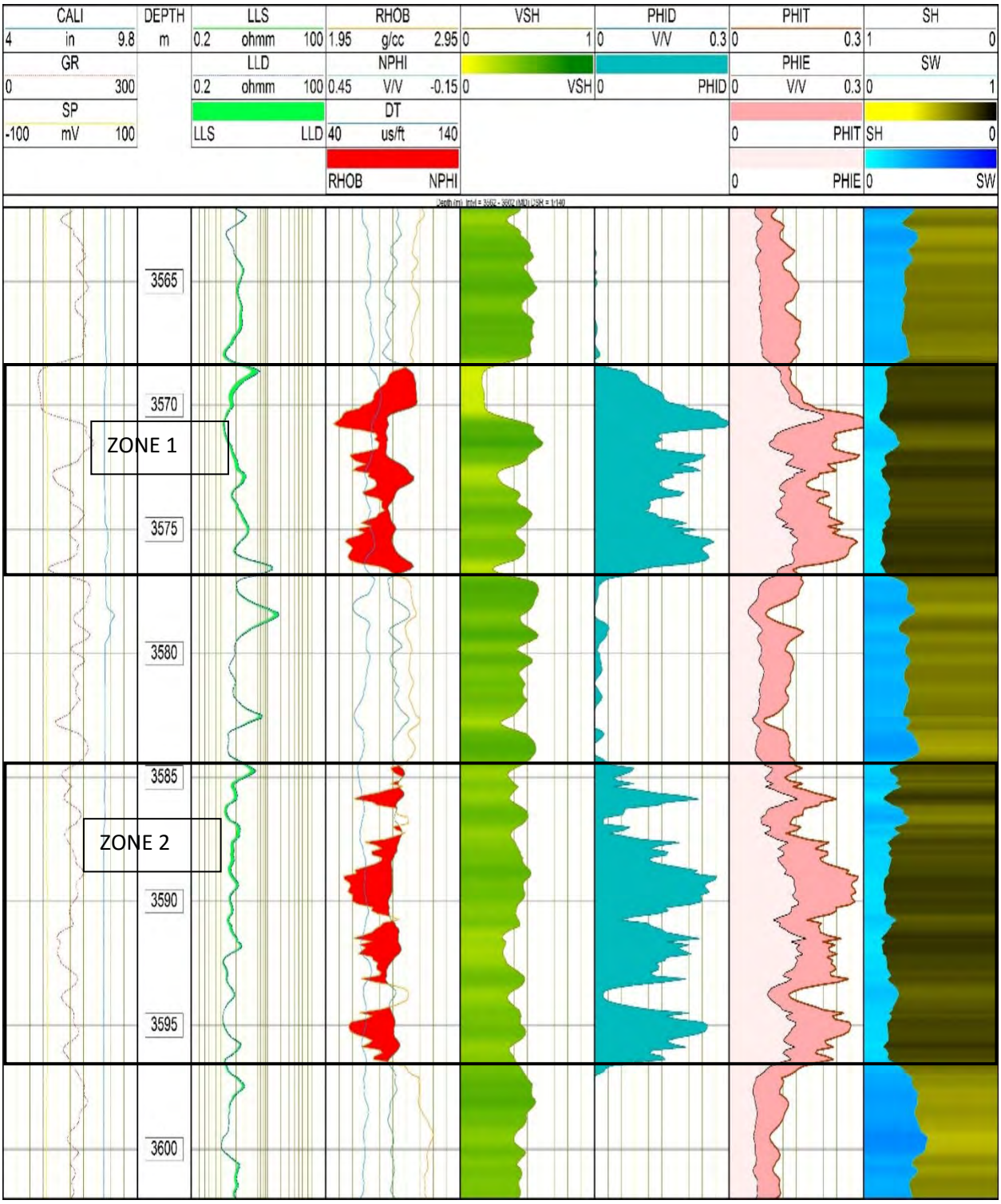

Figure 4.3 Interpreted section of Tajjal-01 well in the C interval, where possible C sands presence can be confirmed with low volume of shale and high porosity, with two zones of interest identified with zone 1 have a net pay of 8m, while zone 2 having a net pay of 11m, marked in black and blue box respectively, and interpreted on PowerLog software.

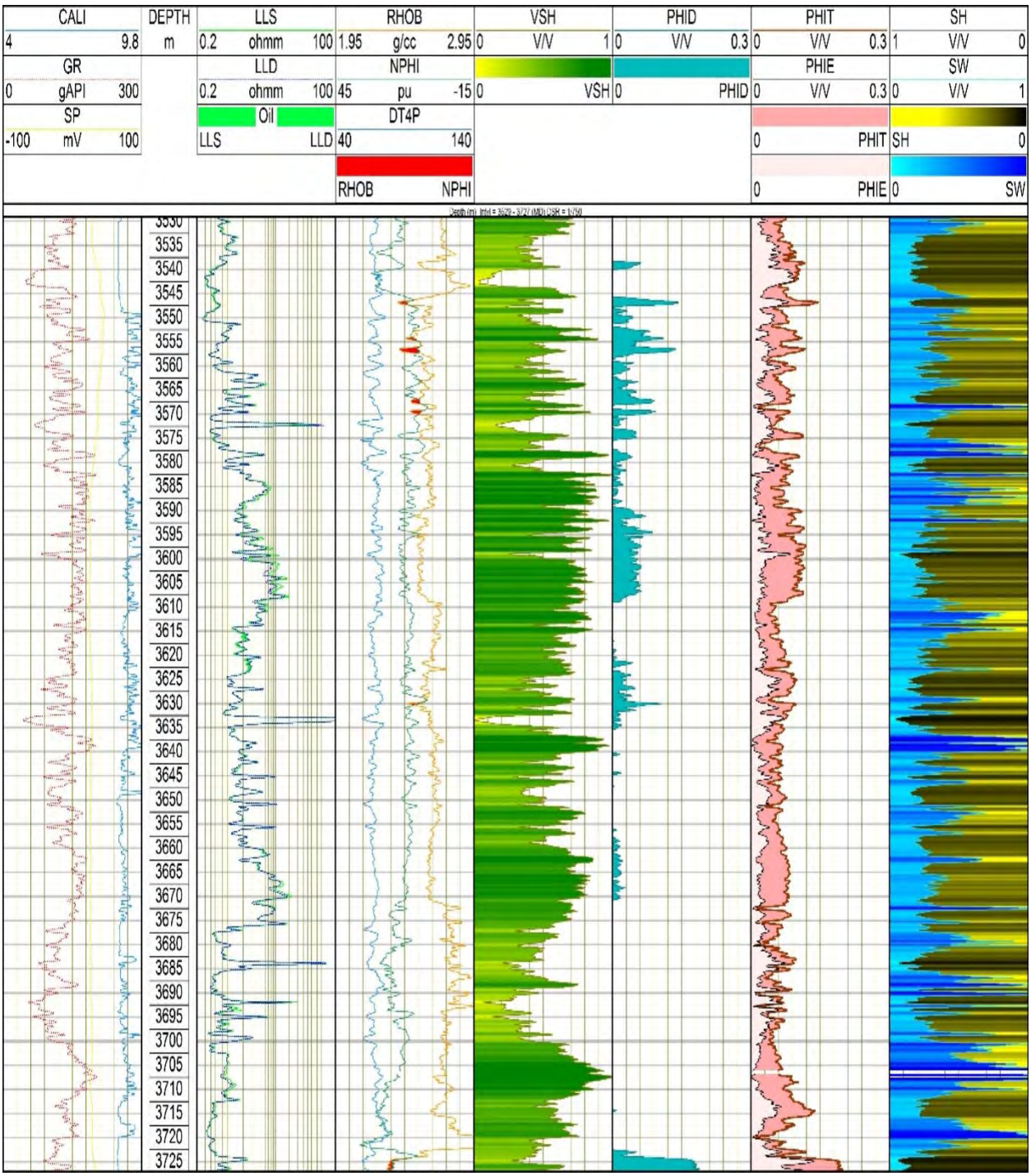

Figure 4.4 Interpreted section of C sands in Tajjal-02 well, where no possible zone of interest was marked, with little indication of hydrocarbon presence and a high water saturation and high volume of shale content for the whole C interval, with interpretation done utilizing PowerLog software.

CHAPTER 05

ROCK PHYSICS MODELLING

5.1 Introduction

Interpretation carried out on seismic is a basic model of identifying traps and reservoir location in subsurface, while further crude information of the reservoir being hydrocarbon bearing can be obtained from petrophysical analysis, yet the qualitative interpretation of the reservoir is not enough to characterize the heterogeneity present in earth. Seismic volume has a large scale of coverage thus the minor details that can be used to quantify the characteristics are often skipped but can be validated using well log data through rock physics modeling that can not only quantify reservoir characteristics but also quantitative properties regarding impedance contrasts. An integration of certain mathematical tools and rock physics models help in reduction the uncertainty of the data. Accurate prediction of elastic properties can be made sure by application of probability distribution rather than using constant values as input. This methodology is helpful for defining analytical solutions of rock physics model, where random variable inputs that are unknown, but the probability distribution is certain, and the uncertainty in the rock physics modeling can further be quantified using probability distribution (Grana and Dvorkin, 2011).

There are numerous developments of rock physics modeling that link the seismic properties to the reservoir but are constrained by lithology, pore fluid, texture, porosity, and saturation of the rock body. To further enhance the complexity that make rock physics more challenging yet more accurate are the greater number of parameters than seismic, thus no unique set of solution can be determined to the given problem. To enable geoscientists to validate several models for a given data set modeling procedures can be used, providing with more robust parameters that can be combined to make reservoir predictions (Grana and Dvorkin, 2011).

5.2 Rock Physics Modelling

Firstly, the characteristic of the reservoir is of key importance on which the rock physics model should be based for the certain reservoir and with its lower and upper bounds characterized accordingly. The Hashin-Shtrinkman-Walpole and Voigt-Reuss bounds are helpful in constructing precise bounds on the maxima & minima an isotropic, linear elastic lithology's effective bulk and shear moduli can be predicted. The Hashin-Shrinkman-Walpole bounds for a

combination of the two elements can be written as shown. in Equation 5.1 and 5.2 (Mavko et al., 2009):

$$K^{HS\pm} = K_1 + \frac{f_2}{(K_2 - K_1)^{-1} + f_1\left(K_1 - \frac{4}{3}\mu_m\right)^{-1}} \tag{5.1}$$

$$\mu^{HS\pm} = \mu_1 + \frac{f_2}{(\mu_2 - \mu_1)^{-1} + f_1\left[\mu_1 + \frac{1}{6}\mu_m\left(\frac{9K_m + 8\mu_m}{K_m + 2\mu_m}\right)\right]^{-1}} \tag{5.2}$$

where, subscripts 1 and 2 refer to the two components of properties with bulk and shear moduli and volume fractions.

These bounds help in characterizing the mixture of minerals and pore fluids, where the upper bounds where bulk and shear moduli are at maximum and when these moduli are at minimum yield the lower bounds respectively (Mavko et al., 2009). Modified Hashin-Shtrinkman-Walpole equations can be constructed based on the above equations to pronounce mixture a mineral with critical porosity and an unconsolidated fluid-solid suspension (Mavko et al., 2009). These modified equations have been helpful in describing clean sandstones using their elastic moduli that evolve over diagenesis processes of compaction and cementation (Mavko et al., 2009). Although these bounds are not rigid bounds, on elastic properties of clean sands as sandstone moduli are often observed to lie above or below it. Spherical porosity is often an idealized representation of grains present in unconsolidated and poorly consolidated sands, providing a geometric relation of porosity and a function of packing and sorting (Mavko et al., 2009).

5.3 Effects of Fluid Saturation

Although dry rock properties are much easier to pronounce but the main effect for viscoelastic parameters is a higher complexity, but more helpful in characterizing the reservoir functions, as a check by primary and shear velocity; a function of the distinctive pressure and serve as an excellent indicator of fluid saturation influence (Han and Batzle, 2004).

Buk modulus is more sensitive to water saturated sandstones in contrast to shear modulus, and as a seismic wave passes it causes increase in the pressure of the pore fluid and volume change of the pore, which raises the rock frame stiffness, hence, raising the bulk modulus. On the contrary shear modulus does not provide any distinct influence on pore fluid or volume change.

Therefore, it can be concluded that any effect on fluid-saturation must be coincided with change in bulk modulus (Han and Batzle, 2004).

Results for poorly consolidated C sands using the Gassman's fluid substitution to determine change in velocity of the fluid saturated pores and to rectify the mixed lithology and differentiate the shales and sandstone lithologies using modified Hashin-Shtirnkman bounds the results of the various cross plots are combined using different conditions.

5.4 Rock Physics Crossplots

5.4.1 Vp vs Vs

In Figure 5.1 the first cross plot well log data at background was utilized with the volume of shale standardized to categorize the sands and shales apart in the C interval, depending on the longitudinal and shear wave velocities. A generalized idea is that both the two parameters show strong positive relation, but in the current scenario the clusters of the data value show a high deflection away from the trend, with the sands shown in yellow and shale in red. The primary velocity for the sands is comparatively lower than of a water or oil saturated sands, with the shaly cluster relatively below the sands, indicating that the sands in C interval in isotropic conditions as gas saturated in well Tajjal-01 displayed in Figure 5.1. Similarly, the same crossplot for well Tajjal-02 was plotted, although the clusters showed a good fitting on the general trend line, but the trend line moved very back with very low velocities, and no deflection by sands or shale facies, thus can be concluded that in Tajjal-02 the sands are water saturated displayed in Figure 5.2.

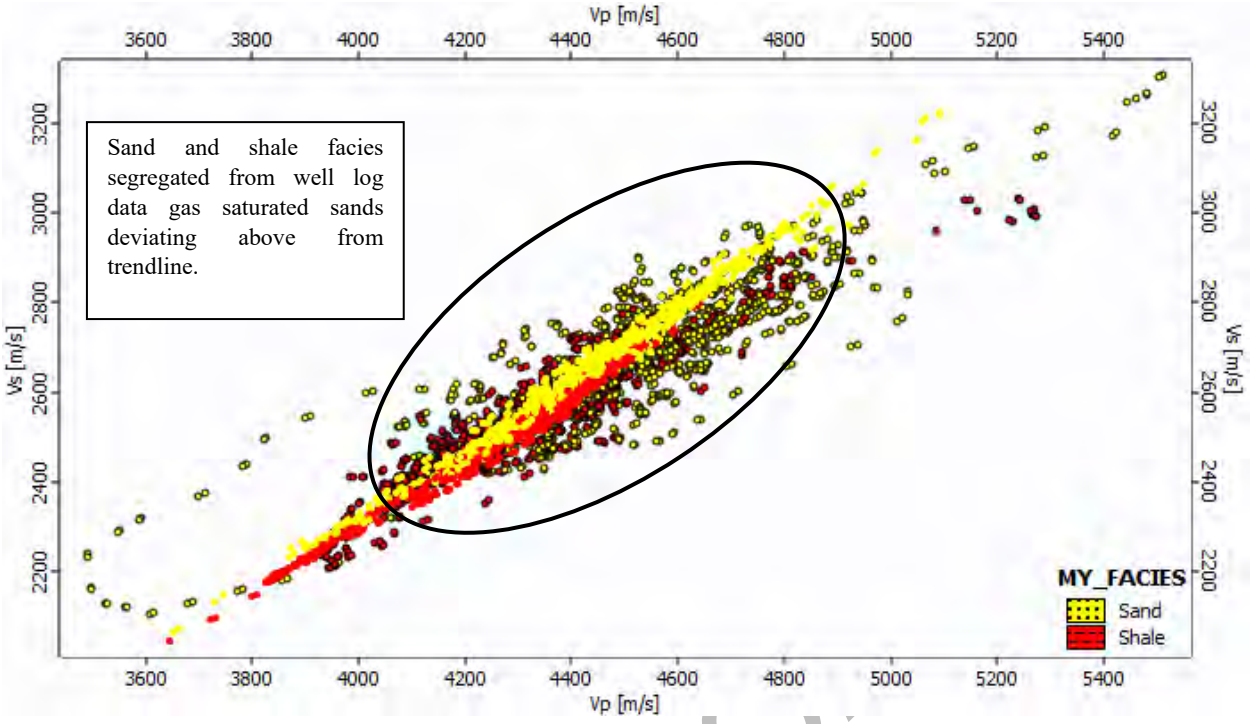

Figure 5.1 Rock physics crossplot between Vp and Vs for Tajjal-01 well, utilizing Hampson and Russell (HRS) software.

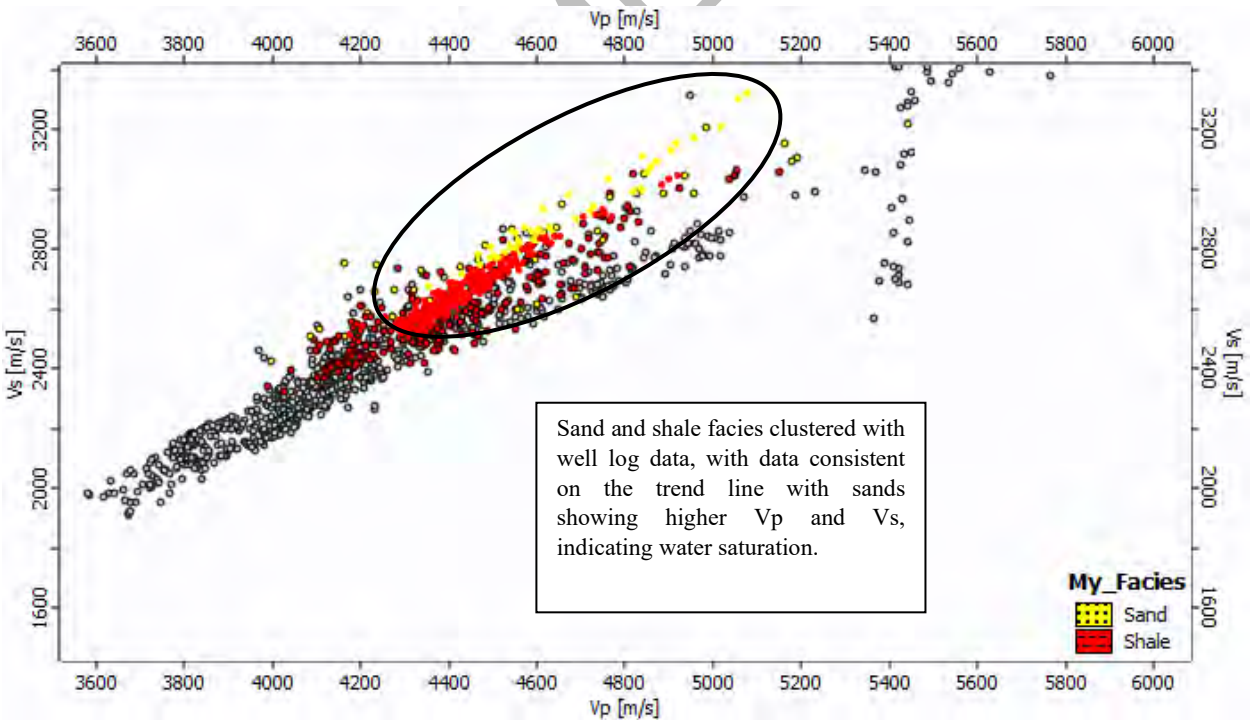

Figure 5.2 Rock physics crossplot between Vp and Vs for Tajjal-02 well, utilizing Hampson and Russell (HRS) software.

5.4.2 Vp vs Density

For further validation of results another crossplot to distinguish sand shale facies in the C interval and to correlate the results of the above crossplot, the Vp relation with density was plotted, with results of crossplot in Figure 5.3 of Tajjal-01, in which the trend of well log data highly clustered on the trend line, with shale facies distinguished having low compressional velocity and moderate density due to compaction, but sands of the C interval being of low density and low velocity, that correlates to the Vp versus Vs crossplot being gas saturated. Crossplot using same template run on well log data of Tajjal-02 however yielded results displayed in Figure 5.4, that were away from trend line and the clusters of the sands with relatively high velocities, and densities, then that of Tajjal-01 well, and it concludes also that the C interval in Tajjal-02 well are highly water saturated.

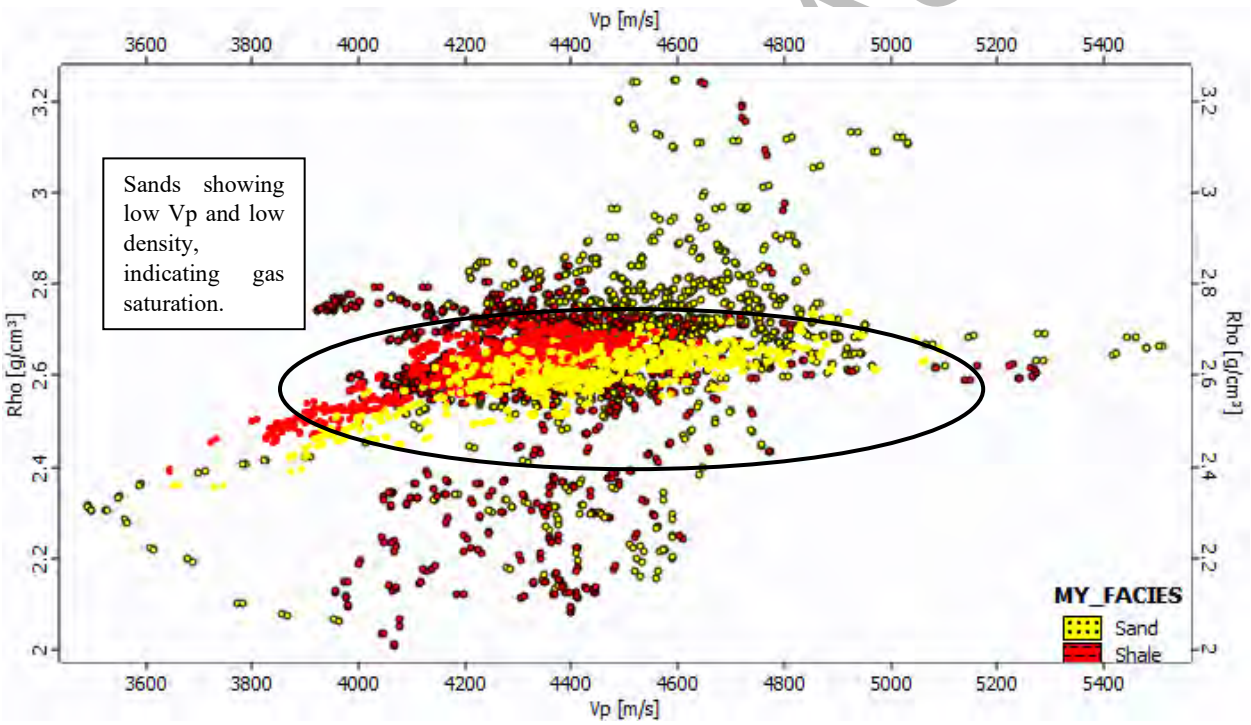

Figure 5.3 Rock physics crossplot between Vp and density for Tajjal-01 well, utilizing Hampson and Russell (HRS) software.

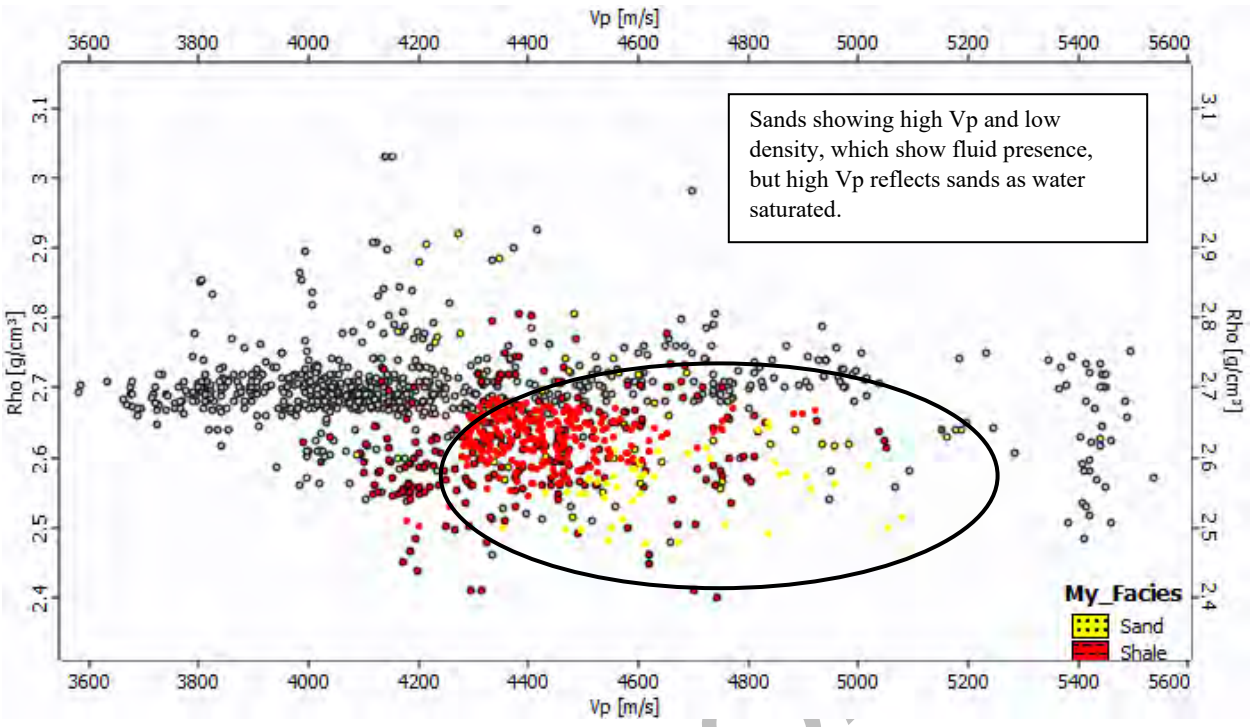

Figure 5.4 Rock physics crossplot between Vp and density for Tajjal-02 well, utilizing Hampson and Russell (HRS) software.

5.4.3 Acoustic Impedance vs VP/VS ratio

A key and most crucial crossplot template in any rock physics analysis is one between acoustic impedance and Vp/Vs ratio, that helps in determining valuable information about the reservoir, with assurance that can be correlated more precisely with Vp vs Vs crossplot providing further confidence. The crossplot in Figure 5.5 being of Tajjal-01 well, shows the well log data cluster at a very low Vp/Vs ratio, but the interesting fact is that we find that the discrimination of clay content using Vp/Vs would represent a similar resolution as compared to the acoustic impedance where we see that the trend would change with increasing porosity, and seems to appear much more difficult. Of our rock physics template keeping in mind the low GR response with depth and lower acoustic impedance the rock body not only yields lesser clay content but also a higher proportion of gas saturation in the sands, with shale representing higher Vp/Vs ratio value and slightly lower acoustic impedance. In Figure 5.6 the well log data, is clustered at a high Vp/Vs ratio, but the sand facies show relatively lower Vp/Vs ratio than Tajjal-01 well crossplot, and slightly higher acoustic impedance that conclude once again that the Tajjal-02 well highly water saturated, and further strengthening the confidence of our petrophysical analysis.

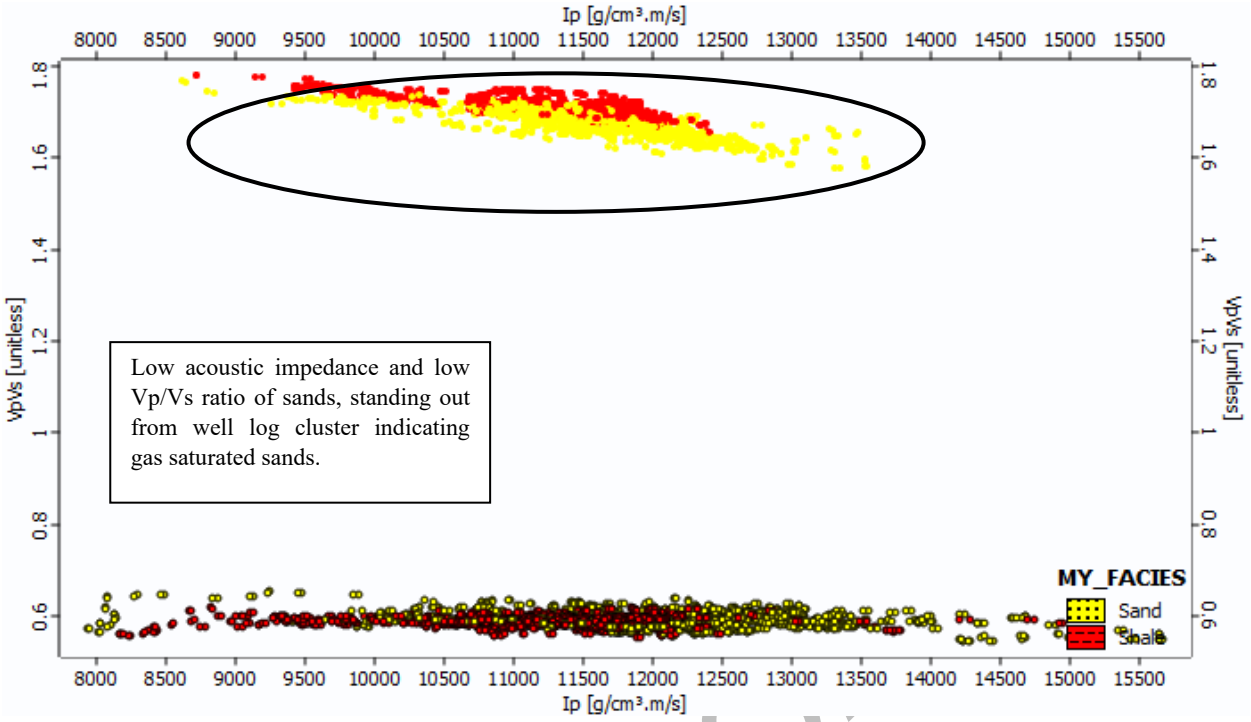

Figure 5.5 Rock physics crossplot between acoustic impedance and Vp/Vs for Tajjal-01 well, utilizing Hampson and Russell (HRS) software.

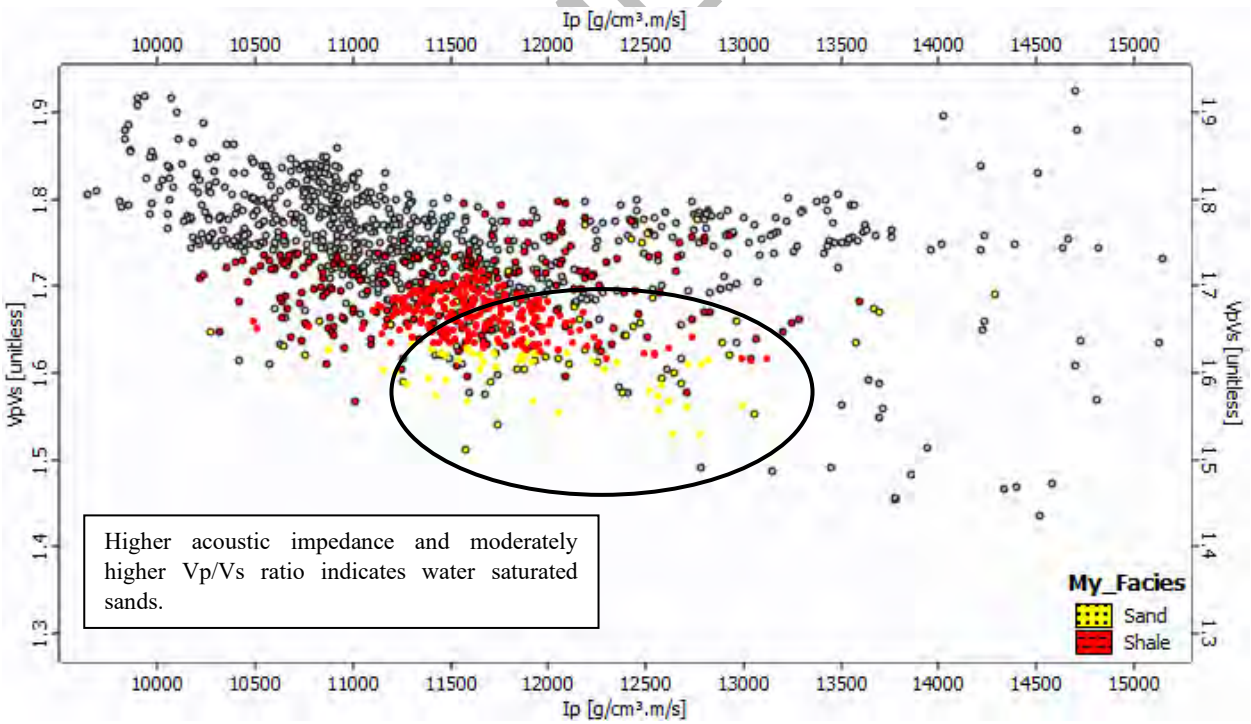

Figure 5.6 Rock physics crossplot between acoustic impedance and Vp/Vs for Tajjal-02 well, utilizing Hampson and Russell (HRS) software.

CHAPTER 06

SESIMIC POST STACK INVERSION

6.1 Introduction

Rock physics analysis can be characterized as the first stage of reservoir characterization, but with enhanced quantitative analysis of reservoir rock properties, the results are confined to the well. To spatially distribute the observed calculations and characterize the reservoir on the grid the results generated by rock physics are then used as an input source, and by applying seismic inversion that helps in transforming the seismic interface properties in layered properties, spatial characterization and quantification of the reservoir can be observed. (Yilmaz, 2001; Ashcroft, 2011). Generalized workflow that was followed has its basis on Ali et al., (2018). The study was done based on generation of attributes using Vp, Vs and density as anticipated by Goodway et al., (1997) the lambda-mu-rho technique originating from studies of compacted rock areas. The lambda-mu-rho and model-based inversion techniques were applied in this study (Russell and Dommico, 1988), which are a characteristic of deterministic inversion approach.

6.2 Model-Based Inversion

Inversion has its origin characterized in the basic convolutional model, and by inverting that model, one can attain the reflectivity series, which can be further utilized to quantify layer properties. Model-based inversion is a broadband technique that builds an initial impedance model driven by well log data combined with the velocity information, and horizon information extracted from seismic (Toqeer et al., 2021). The initial acoustic impedance model is changed by comparing with the original seismic data, and the model is iterated and updated until misfit between seismic data and the synthetic seismogram that is obtained by convolving wavelet with the acoustic impedance model is removed. (Veeken, 2007; Simm and Bacon, 2014; Ashcroft, 2011). At first the well to seismic tie is performed for horizon marking, and well data is used to construct the initial earth model incorporating the low frequency trend, upon which a low frequency model is generated through well logs, and the horizons interpreted from seismic horizons. This is done to better characterize the stratigraphic features as more realistic and create a better geological model, to achieve the targeted realistic inverted impedance (Li and Zhao, 2014). A point of key concern to be mentioned is that the seismic data is bandlimited, thus low

frequencies do not form part of the signal spectrum, and without these low frequencies the prediction of reservoir properties is not unique and uncertain (Sams and Carter, 2017).

An acoustic impedance profile is generated through seismic inversion thus characterizing desired reservoir properties such as porosity, and for model-based inversion, the method starts by generating an initial geological model of earth and incorporating low frequency model from well log data, which further is iteratively checked in contrast the seismic data. Comparisons of the observed and calculated model is checked through forward modelling and the error is checked, and iterations occur till the uncertainty is removed, after which they stop.

In the study to characterize sands in C interval and their potential two profiles were generated on the inline 1454, where the Tajjal-01 well is located, where the first geological model was generated using the P-wave velocities of Tajjal-01 well displayed in Figure 6.1, to generate an acoustic impedance profile, which yielded a 99% correlation with the seismic data. Impedance scale varied from a maxima 16,000 ((m/s)*(g/cc)), with purple hue to a minima of 10,039 ((m/s)*(g/cc)) having green color displayed in Figure 6.2 below. The sands of C interval fell in the range of 10,411 ((m/s)*(g/cc)) to 11,653 ((m/s)*(g/cc)) forming a light green to sharp yellow color, which showed a very low acoustic impedance indicating higher porosity and sands being gas saturated, which was a validation to the rock physics results, and these reservoir properties were then spatially distributed to characterize the hydrocarbon bearing gas saturated C sands as displayed in Figure 6.3.

A second profile was constructed using the shear wave velocity to generate a shear impedance profile on the Tajjal-01 well containing inline, with the same 99% correlated geologic model the shear impedance profile was generated. The profile displayed in Figure 6.4 shows the maxima at 8000 ((m/s)*(g/cc)) with a purple color and the minima at 6000 ((m/s)*(g/cc)) with green color. Since shear wave has no effect on fluids and specially if the formation is gas saturated, it does yield low impedance values that give only slight hint but does not generate a certainty as the acoustic impedance profile. The sands of C interval showed a color range of dull yellow to orange color with the dull yellow color being the lowest shear impedance shade, with a value of 6667 ((m/s)*(g/cc)) and orange shade being 6833 ((m/s)*(g/cc)). Although not a very considerable result but it does show the effective media being porous and holds our acoustic

impedance profile in Figure 6.2 valid, the slice of the shear impedance value spatially mapped for the reservoir is shown in Figure 6.5.

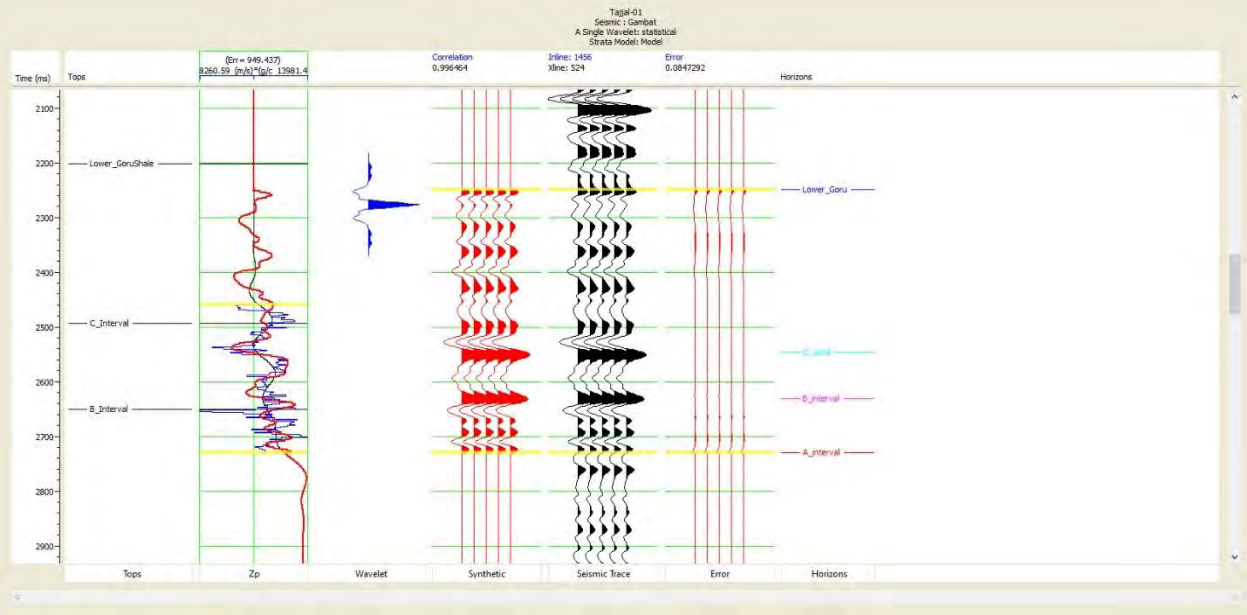

Figure 6.1 Statistical wavelet convolved with the extracted low frequency induced calculated geological model of the area for minimising the uncertainty between calculated and observed models, with a 99% correlation was achieved using Hampson and Russell (HRS) software.

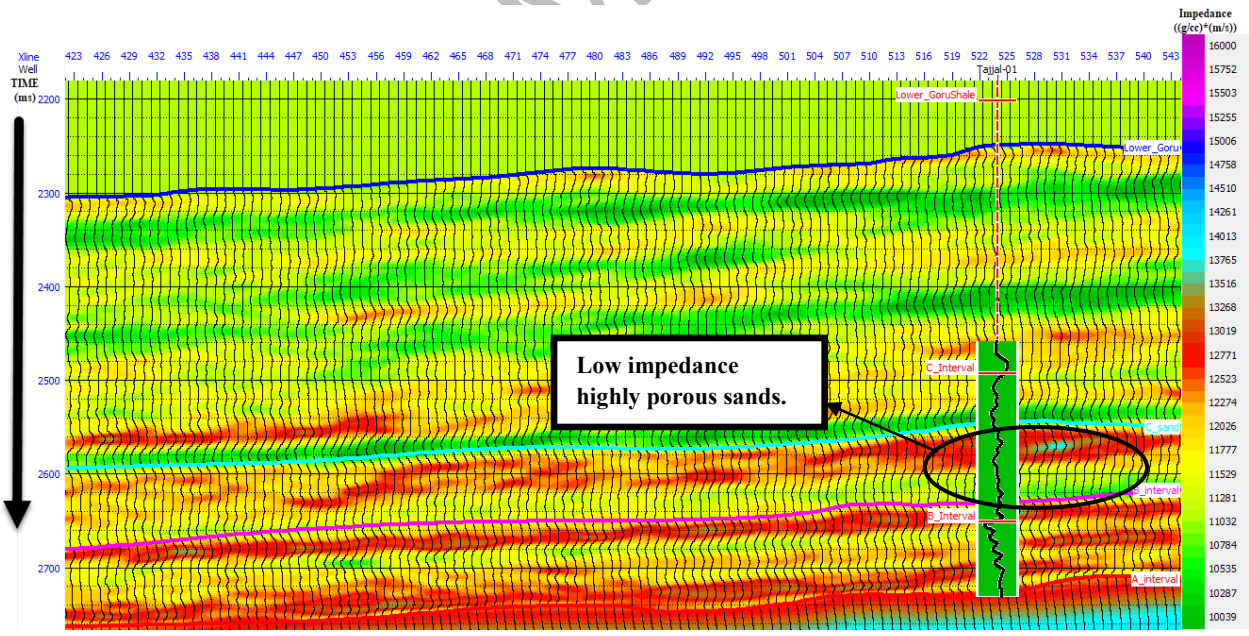

Figure 6.2 Cross section view of inline 1454 displaying the acoustic impedance contrast of lithologies highlighting highly porous zones which was created using Hampson and Russell (HRS) software.

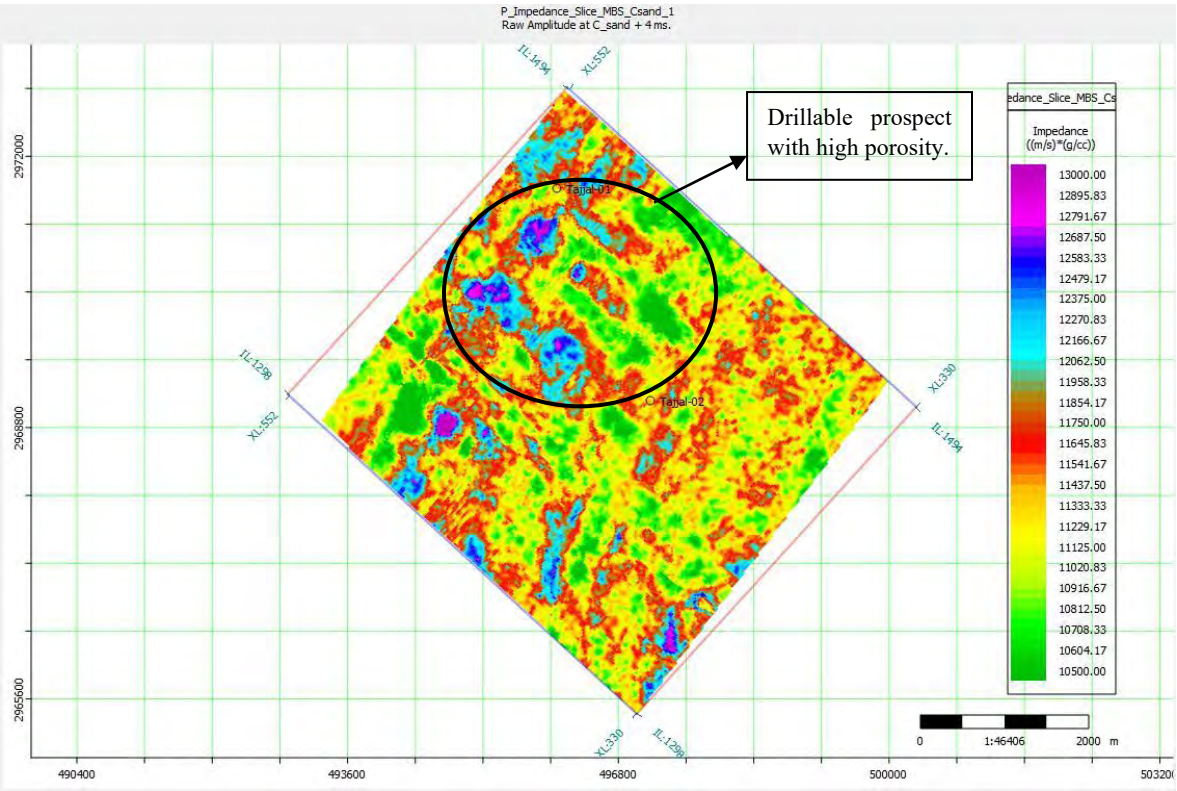

Figure 6.3 Spatial distribution of low acoustic impedance profiles of C sands marking areas of low impedance and high porosity with green colour, potential prospect areas for future drilling, achieved using Hampson and Russell (HRS) software.

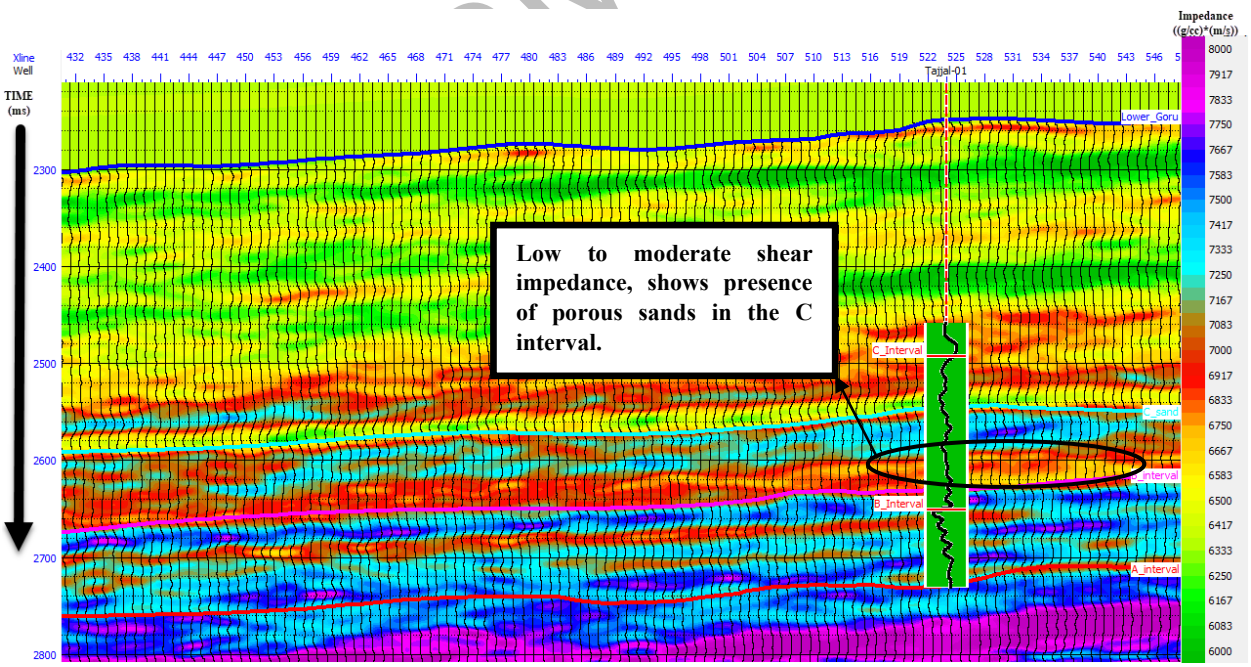

Figure 6.4 Cross section view of inline 1454 displaying the shear impedance contrast of lithologies with low impedance as sands, created using Hampson and Russell (HRS) software.

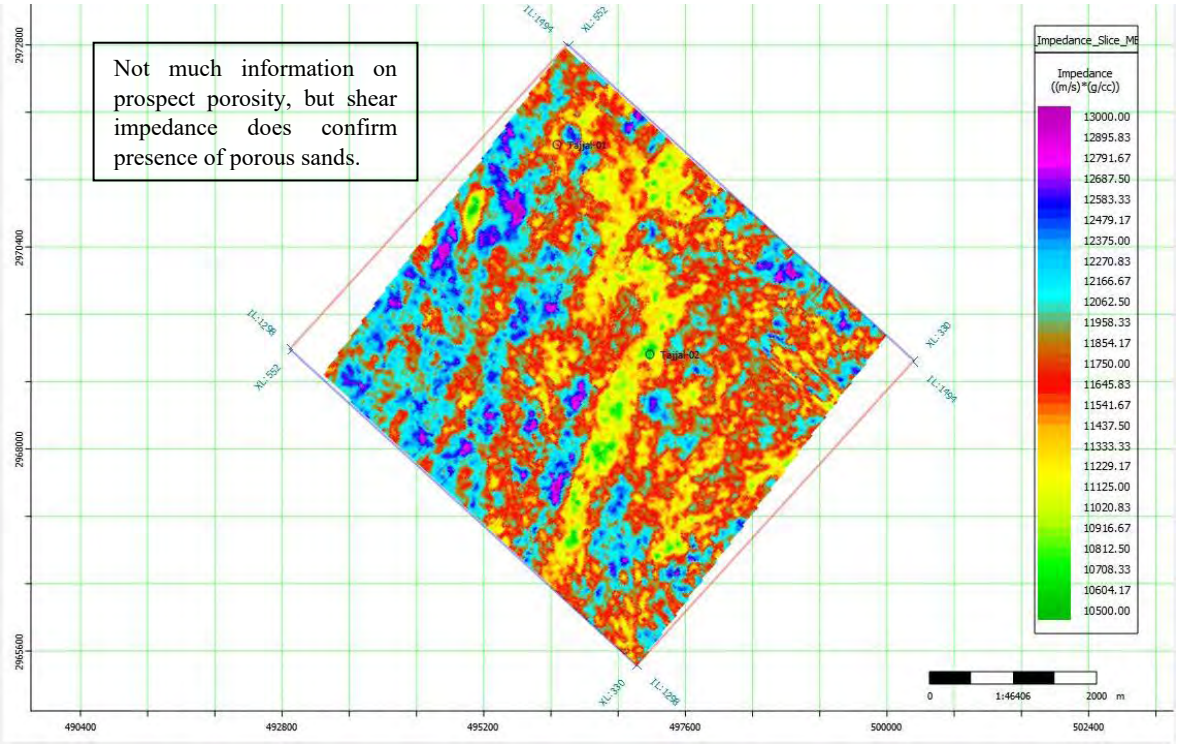

Figure 6.5 Spatial distribution of shear impedance profiles of C sands marking areas of moderate red to yellow colour as sand present areas as shear modulus does not pass-through fluids, achieved using Hampson and Russell (HRS) software.

6.3 Lambda-Mu-Rho Inversion

A more robust methodology is utilizing the rock physics analysis and inversion workflows in combination is by transforming the model-based inversion output volume int Lambda-roh and Mu-rho and Vp/Vs ratio volume. The objective of this analysis is to determine the feasibility of segregating the reservoir facies and carrying out the imaging of the reservoir architecture with seismic attributes. Goodway et al., (1997) proposed the Lambda-Mu-Rho in which the Lambda and Mu parameters were introduced using Lame's parameter (λ and μ) and density are prime components of the new simultaneous inversion approach. The Equation 6.1 shows the relation between lambda-rho.

$$\lambda\rho = (\rho V_p)^2 - c(\rho V_p)^2 \qquad (6.1)$$

where, Vp, Vs and ρ are P-wave velocity, S-wave velocity, and density, while c is a constant that is equal to 2. Russell et al., (2003) proposed that if the well log data is available than c for a given basin setting can be locally determined. The effect of fluid computation is influenced by the constant c, variable for different geological environments. Value of c falls within the range

set by Dillon et al., (2003) that is applicable for both offshore and onshore. Mu-rho is the square of S-wave impedance representing rigidity (rock matrix) given by the equation 6.2.

$$\mu\rho = (\rho V_s)^2 \quad (6.2)$$

The Lambda-Mu-Rho inversion is a powerful technique that can help in characterizing reservoir lithology and fluid distribution of sands in C interval in Gmabat-Latif block. Figure 6.6 displays the profile image of the lambda-rho attribute applied on the inline 1454 of Tajjal-01 well where the lambda-rho property is more susceptible to the pore fluids, with the maximum range having a purple color and value of 60 (GPa*g/cc), and a minimum represented by green color and a value of 20 (GPa*g/cc). Since more sensitivity to pore fluid, inversion results show a thick lithology of low impedance values with light green color with a range of 22.5 to 26.7 (GPa*g/cc), confirming the presence of gas saturated sands in the C interval, and spatial distribution is given in time slice displayed in Figure 6.7.

The Mu-rho property is sensitive to the rock matrix with a maximum to minimum range of 69.9 to 35.1 (GPa*g/cc), color varying from green (minimum) to purple (maximum). The cross section of the inline 1454 is displayed in Figure 6.8, where the rock matrix distinguished by mu-rho attribute is in a golden yellow color with a value range of 43.8 to 45.9 (GPa*g/cc), which is thicker in contrast to the sands identified by lambda-rho, but since it depends upon matrix rigidity, so pore fluids are more susceptible to response from lambda-rho. The spatial distribution of sands of C interval is displayed in Figure 6.9.

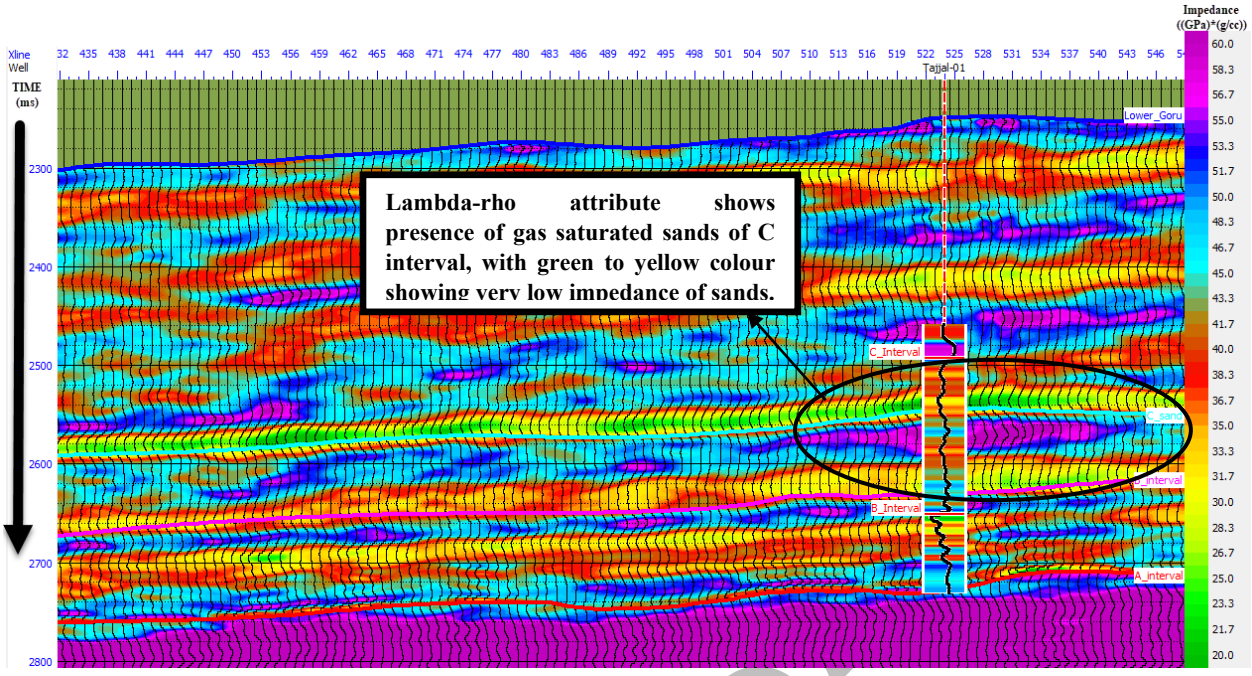

Figure 6.6 Lambda-rho attribute applied to Tajjal-01 well, an attribute much sensitive to fluid presence indicates low acoustic impedance highlighted with green to yellow colour as reservoir sand being highly gas saturated, created using Hampson and Russell (HRS) software.

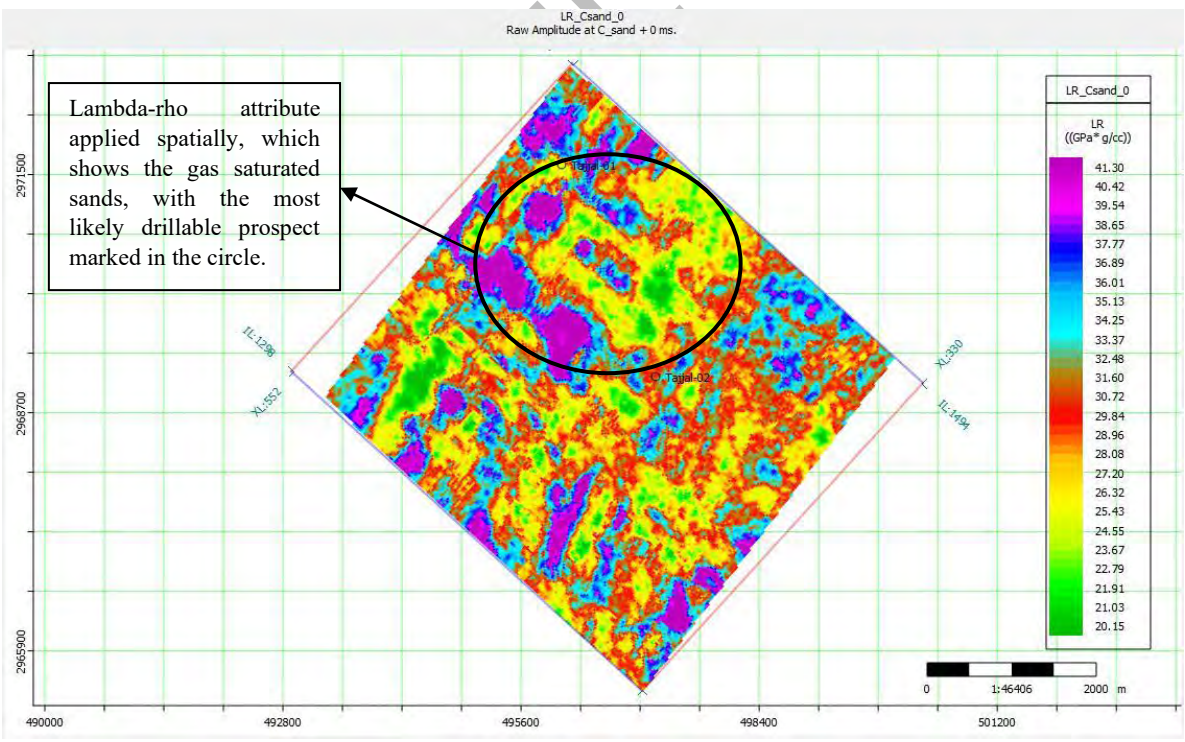

Figure 6.7 Spatial distribution of the acoustic impedance utilizing lambda-rho attributes, indicating similar pattern to model-based inversion spatial distribution but more refined to gas saturated reservoir sands, created using Hampson and Russell (HRS) software.

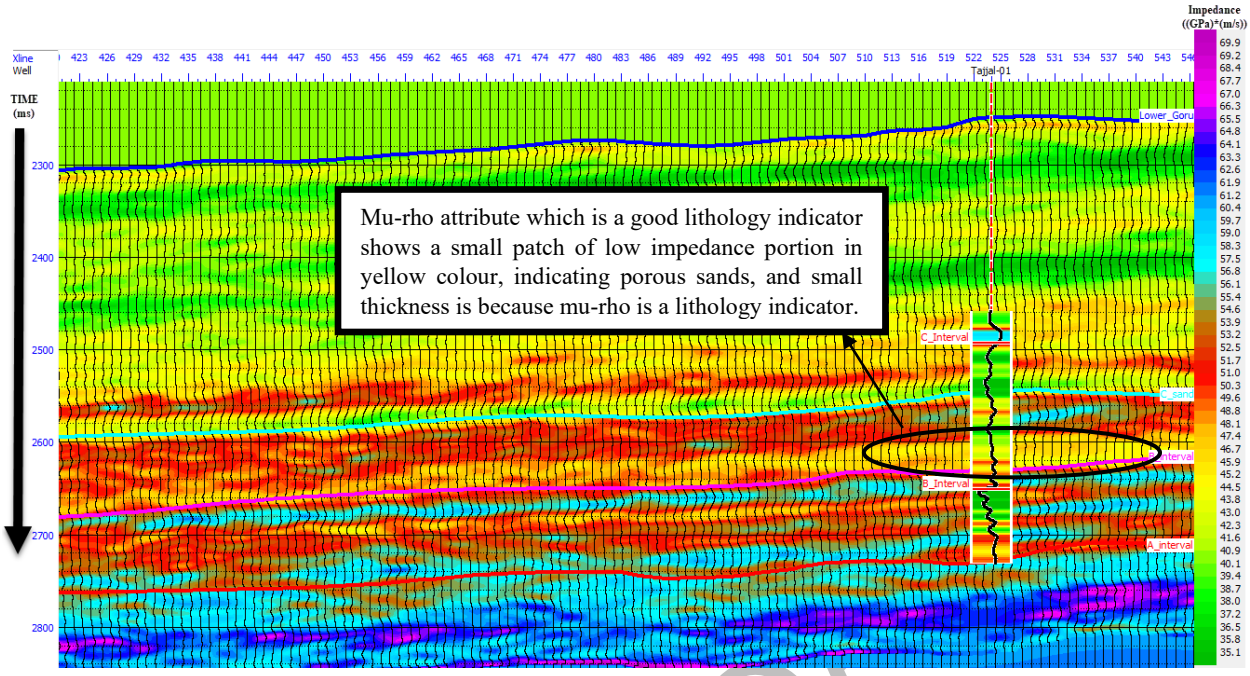

Figure 6.8 Mu-rho attribute applied to Tajjal-01 well, an attribute much sensitive to rock matrix indicates low acoustic impedance highlighted with green to yellow colour as reservoir sand being porous sand bodies, created using Hampson and Russell (HRS) software.

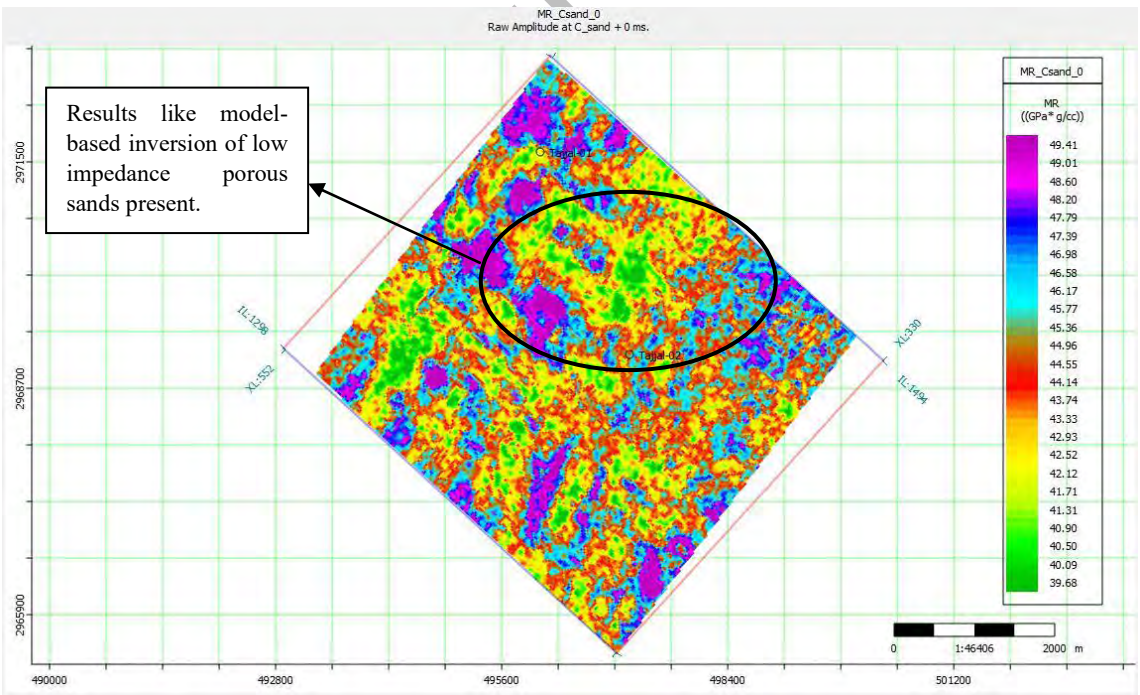

Figure 6.9 Spatial distribution of the acoustic impedance utilizing mu-rho attributes, indicating similar pattern to model-based inversion spatial distribution highlighting porous sand bodies, identified by yellow to green colour created using Hampson and Russell (HRS) software.

6.4 Comparison of Inversion Techniques

The results as input parameters from rock physics with log conditioning were helpful in quantifying properties, but spatial distribution in block of reservoir characteristics were still an ambiguity. Inversion was a useful tool in filling the gaps of spatial distribution of reservoir characteristics, and it cannot be judged that which inversion technique was more superior to the other, because of the basic quantification each technique brought was useful in characterizing reservoir in its own method, but the lambda-mu-rho inversion had a slight edge over model-based inversion. Model-based inversion which used the seismic volume and well logs, for generating an earth model that was close to the observed model, with low frequency algorithms was very useful in identifying the spots of low impedance, in which acoustic impedance was more susceptible to identifying fluid changes, but it did validate the spatial distribution of low impedance high porosity zones in the study area. The lambda-mu-rho inversion technique is a more powerful tool that utilizes key properties of reservoir architecture in which lambda-rho is sensitive to pore fluid, and in our case very helpful in identifying spots where gas saturated sands were present with low impedance values, whereas the mu-rho attribute which gives information about rock matrix had somewhat similar results to the shear impedance model-based inversion results, and characterized spatial presence of sands in C interval.

CHAPTER 07

DISCUSSIONS AND CONCLUSIONS

7.1 Discussions

The study was focused on the characterization of the reservoir sands that are present in the mixed facies of the C interval, in the Gambat-Latif block of the Lower Indus Basin, in the south of Pakistan. The study was characterized into stages from seismic structural interpretation and identification of the horizons in subsurface, after which petrophysical analysis were to determine presence of hydrocarbon footprint in the well data, on which the basis of reservoir characterization was laid out to better quantify the reservoir properties. The quantification of the reservoir in rock physics modelling was since based on well log data, the spatial distribution and further correlation was done utilizing inversion techniques to spatially map the reservoir quantitative properties using two different inversion techniques.

The study area is very potentially rich since there are major discoveries in surrounding blocks, of gas and oil. There have been different studies carried out by in the study area, but quantification of reservoir properties has been sparse, with most of the case scenarios run on isotropic fluid substitution, with changes observed in the crossplots on basis of gas and water saturation. The study was firstly conducted by identifying subsurface structure in the study block, that showed horst and graben structures, with the fault architecture being of synthetic faults, having no antithetic faults associated with fault trends in the NW-SE. The structure was much shallower in the western part of the study block, and got deeper in the east, which was observed in the values of time and depth contour maps.

After preliminary identification of the subsurface structure and depths associated with it, well data from the wells Tajjal-01 and Tajjal-02 underwent petrophysical evaluation, to locate zones of hydrocarbon accumulation in the study area. As the primary target for the study was the sands of C interval, the petrophysical evaluation, yielded two zones of interest having a higher rate of hydrocarbon accumulation with zone 1 yielding the highest saturation of hydrocarbon of 81.7%, and zone 2 showing hydrocarbon saturation of 80.5%, while the Tajjal-02 well as highly water saturated, yielded no high confidence.

Although petrophysical evaluation did confirm Tajjal-01 as being hydrocarbon bearing and sands of C interval that could be coupled further with other sands of Lower Goru as high prospective

targets, a further advanced step taken to correlate the petrophysical analysis with well data by quantifying the reservoir characteristics on basis of quantitative properties of impedance, Vp/Vs ratio, and density was checked. Log conditioning was applied for quality assurance of input data. The rock physics model that was used based on the modified Hashin-Shtrinkman bounds and keeping the reservoir sands as unconsolidated or poorly consolidated sands, due to presence of mixed facies in the C interval, quantitative properties were derived. Three major crossplots were defined to further characterize the well data of Tajjal-01 and Tajjal-02 wells. The Vp and Vs crossplot showed the Tajjal-01 well clusters which not only distinguished the sand and shale facies as deflection away from trend line as an indication of gas saturated sands and lower Vp and much lower Vs values for sands and slightly higher for shales, whereas the Tajjal-02 well was clustered on the trend line and having higher Vp and Vs low Vs values falling in the water saturated region. The crossplot of Vp and density on the other hand further validated the response of Tajjal-01 well with high gas saturation yielding low Vp and density values for sands, and in Tajjal-02 the Vp was slightly lower in contrast to Tajjal-01 but density was higher as the case of water saturation. The final crossplot of acoustic impedance and Vp/Vs ratio was the final validation from well data lower acoustic impedance the rock body not only yields lesser clay content but also a higher proportion of gas saturation in the sands, with shale representing higher Vp/Vs ratio value and slightly lower acoustic impedance. The well log data, being clustered at a high Vp/Vs ratio, but the sand facies show relatively lower Vp/Vs ratio than Tajjal-01 well crossplot, and slightly higher acoustic impedance that conclude once again that the Tajjal-02 well highly water saturated.

Final characterization of reservoir properties was done using inversion techniques that combined both the well log data and the seismic data volume. Two different inversion techniques were applied to quantify the reservoir characteristics, in which model-based inversion yielded an almost similar geologic model as the observed, and displayed areas of low acoustic impedance as porous sand facies, where further drop in the impedance indicated hydrocarbon presence in light green color. Unlike the model-based inversion that only provided an impedance contrast basis of quantification, the two different attributes namely lambda-rho and mu-rho were susceptible to different sets of information, in which lambda-rho which is more sensitive to the pore fluid presence in the porous media, while mu-rho better characterizes the rigidity of the rock matrix. The lambda-mu-rho inversion with the two attributes applied differently on the seismic inverted

volume, where the lambda-rho confirmed gas saturated sand facies on inline 1454 using Tajjal-01 well and were spatially distributed on time slice, while the mu-rho attribute identified the sand facies on inline 1454 with combination of Tajjal-01 well and then spatially spread out on the data set. The lambda-mu-rho inversion provided a higher degree of reservoir characterization than the model-based inversion as a more advanced technique.

7.2 Conclusions

The following conclusions were drawn from this study:

- Structural interpretation of the seismic volume showed horst and graben structures associated with normal faulting present in the subsurface.
- The fault architecture comprised of NW-SE trending faults, with the structure being shallow and thicker in the west and deeper and thinning to the east.
- Petrophysical evaluation yielded two possible zones of interest in the Tajjl-01 well, with 81.7%, and 80.5% hydrocarbon saturation, whereas Tajjal-02 well yielded no such indications on well log combinations and was highly water saturated.
- Validation of the petrophysical analysis was carried out using rock physics modelling to quantify reservoir properties and comparison of the two wells, which confirmed the presence of gas sands in C interval in Tajjl-01 well, while Tajjal-02 well showed a highly water saturated sand presence.
- Model based inversion was used to map the low acoustic impedance of sand facies using well data from Tajjal-01, and spatially mapped in the limits of base map, to mark areas of low porosity.
- Lambda-mu-rho inversion was applied where the mu-rho attribute that identifies rigidity of rock matrix, showed impedance contrast as low and porous which was spatially mapped to highlight sand facies of the C interval.
- Lambda-mu-rho inversion was carried out in which the lambda-rho attribute highlighted pore fluid presence with very low impedance contrast showing presence of gas in the sands and these gas sands of C interval were spatially mapped on the base map.

References

Abbasi, S., Kalwar, Z., and Solangi, S. 2016. Study of structural styles and hydrocarbon potential of Rajan Pur Area, Middle Indus Basin, Pakistan; *BUJ ES 1. 36-41.*

Ali, A., Alves, T. M., Saad, F. A., Ullah, M., Toqeer, M., and Hussain, M. 2018. Resource potential of gas reservoirs in South Pakistan and adjacent Indian subcontinent revealed by post-stack inversion techniques: J. Nat. Gas Sci. Eng. 49 41–55.

Angeleri, G. P., and Carpi, R. 1982. Porosity prediction from seismic data; Geophys. Prospect 30 580–607, https://doi.org/10.1111/j.1365-2478.1982.tb01328.x.

Ashcroft, W. 2011. A Petroleum Geologist's Guide to Seismic Reflection, Wiley–Blackwell.

Asquith, G. B., Krygowski, D., & Gibson, C. R. (2004). Basic well log analysis (Vol.16). Tulsa, OK: American association of petroleum geologists.

Avseth, P., Mukerji, T., and Mavko, G. 2005. Quantitative seismic interpretation: Applying rock physics tools to reduce interpretation risk, Cambridge University Press, https://doi.org/10.1017/CBO9780511600074.

Aziz, M. Z., and Khan, M. R. 2003. A review of Infra-Cambrian source rock potential in Eastern Sindh, an analogue to Huqf Group of Oman. Infra-Cambrian play of Eastern Sindh, Pakistan.

Bacon, M., Simm, R., and Redshaw, T. 2007. 3-D seismic interpretation, Cambridge University Press, https://doi.org/10.1017/CBO9780511802416.

Bjorlykke, K., 2010 Petroleum Geoscience: From Sedimentary Environments to Rock Physics, Springer.

Bosch, M., Carvajal, C., Rodrigues, J., Torres, A., Aldana, M., and Sierra, J. 2009. Petrophysical seismic inversion conditioned to well-log data: Methods and application to a gas reservoir; Geophysics 74 O1–O15, https://doi.org/10.1190/1.3043796.

Bosch, M., Mukerji, T., and Gonzalez, E. F. 2010. Seismic inversion for reservoir properties combining statistical rock physics and geostatistics: A review; Geophysics 75 75A165, https://doi.org/10.1190/1.3478209.

Chen, Q., and Sidney, S. 1997. Seismic attribute technology for reservoir forecasting and monitoring; Lead Edge 16 445–448, https://doi.org/10.1190/1.1437657.

Chopra, S., and Marfurt, K. J. 2007. Seismic attributes for prospect identification and reservoir characterization: Geophysics. Dev. Ser. 11465, https://doi.org/10.1190/1.9781560801900.

Delaplanche, J., Lafet, Y., and Sineriz, B. 1982. Seismic reflection applied to sedimentology and gas discovery in the Gulf of Cadiz: Geophys. Prospect. 30 1–24.

Dillon, L., Schwedersky, G., Vasquez, G., Velloso, R., and Nunes, C. (2003). A multiscale DHI elastic attributes evaluation: The Leading Edge, 22, 1024-1029.

Dobrin and Savit., 1988, Geophysical Exploration, Hafner Publishing Co.

Goodway, B., Chen, T., and Downtown, J. 1997. Improved AVO fluid detection and lithology discrimination using Lame petrophysical parameters; λρ, μρ & λρ/ μρ fluid stack, from P- and S inversions: Presented on 67th Annual international Meeting, SEG Expanded Abstracts, pp. 183–186.

Grana, D. and Dvorkin, J. 2011. The link between seismic inversion, rock physics, and geostatistical simulations in seismic reservoir characterization studies; Lead Edge 30 54–61, https://doi.org/10.1190/1.3535433.

Han, D. H., & Batzle, M. L. (2004). Gassmann's equation and fluid saturation effects on seismic velocities. *Geophysics 69*, no. 2 (2004): 398-405.

Hearts, J. R., Nelson, P. H., and Paillet, F. L. 2002. Well Logging for Physical Properties: A Handbook for Geophysicists, Geologists and Engineers, 2nd edn, John Wiley & Sons, Chichester.

Kadri, I. B. (1995). petroleum geology of Pakistan, Karachi, Feroz sons (pvt) ltd.

Kazmi, A. H., & Rana, R. A. (1982). Tectonic Map of Pakistan, 1:1000000. Geology Survey of Pakistan, Quetta, Pakistan.

Kazmi, A. H., Abbasi, I. A. (2008). Stratigraphy & Historical Geology of Pakistan, Department & National Centre of Excellence in Geology.

Kazmi, A.H & Jan, M.Q, (1997), Geology and tectonics of Pakistan, Graphic publisher, Karachi, Pakistan.

King, D. E. 1990. Incorporating geological data in well log interpretation; In: Geological Applications of Wireline Logs, pp. 45–55, https://doi.org/10.1144/gsl.sp.1990.048.01.06.

Kingston, D. R., Dishroon, C. P., & Williams, P. A. (1983). Hydrocarbon plays and global basin classification. *AAPG bulletin, 67(12),2194-2198.*

Landa, J. L., Horne, R. N., Kamal, M. M., and Jenkins, C. D. 2000. Reservoir characterization constrained to well-test data: A field example SPE Reserv. Eval. Eng. 3 325–334, https://doi.org/10.2118/65429-PA.

Li, M., and Zhao, Y. 2014. Chapter 6 – Seismic inversion techniques. In: Geophysical Exploration Technology Applications in Lithological and Stratigraphic Reservoirs, Elsevier, Oxford, pp. 133–198, https://doi.org/10.1016/B978-0-12-410436-5.00006-X.

Lindseth, R. O. 1979. Synthetic sonic logs – a process for stratigraphic interpretation; Geophysics 44-3, https://doi.org/10.1190/1.1440922.

Liner, C. 2016. Elements of 3D seismology, investigations in geophysics; Society of Exploration Geophysicists, https://doi.org/10.1190/1.9781560803386.

Mavko G, Mukerji T and Dovrkin J 2009 *The Rock Physics Handbook* 2nd edn (New York: Cambridge University Press).

Onajite, E. (2013). Seismic data analysis techniques in hydrocarbon exploration. Elsevier.

Raza, H. A., Ahmed, R., Ali, S. M., Sheikh, A. M., & Shafique, N. A. (1989). Exploration performance in sedimentary zones of Pakistan. Pakistan Journal of Hydrocarbon Research. v.1/1. p.1-7.

Rider, M. H. (1996). The Geological Interpretation of Well Logs; John Wiley and Sons, New York.

Russell, B. H., Hedlin, K., Hilterman, F. J., and Lines, L. R. (2003). Fluid property discrimination with AVO: A Biot-Gassmann perspective: *Geophysics, 68.* 29-39.

Russell, B., and Dommico, S. 1988. Introduction to seismic inversion methods, SEG.

Sams, M., and Carter, D. 2017. Stuck between a rock and a reflection: A tutorial on low-frequency models for seismic inversion; Interpretation 5 B17–B27.

Schlumberger, L. I. (1989) Principles and Application: Schlumberger Wireline and Testin. *Houston, Texas, 21-89*.

Shah, S. M. I. 2009. Stratigraphy of Pakistan. Geological Survey of Pakistan. Memoirs, v.22.

Shah, S. M. I., Ahmed, R., Cheema, M. R., Fatmi, A. N., Iqbal, M. W. A., Raza, H. A., & Raza, S. M. (1997). Stratigraphy of Pakistan. Geological Survey of Pakistan. Memoirs, v. 12, p.137.

Silva, M. Da., Rauch-Davies, M., and Cuervo, A. 2004. Data conditioning for a combined inversion and AVO reservoir characterisation study, 66th EAGE Conf.

Simm, R., and Bacon, M. 2014. Seismic Amplitude: An interpreter's handbook, Cambridge University Press.

Stoneley, R. (1995). Introduction to petroleum exploration for no-geologists. Oxford University Press, USA.

Tittman, J., & Wahl, J. S. (1965). The physical foundations of formation density logging (gamma-gamma). *Geophysics,30(2)*, 284-294.

Toqeer, M., Ali, A., Alves, T. M., Khan, A., & Hussain, M. (2021). Application of model based post-stack inversion in the characterization of reservoir sands containing porous, tight and mixed facies: A case study from the Central Indus Basin, Pakista. *Journal of Earth System Science, 130(2),* 1-21.

Veeken, P. C. H. 2007. Seismic Stratigraphy, Basin Analysis and Reservoir Characterisation, Elsevier, Amsterdam.

Veeken, P. C. H., and Da Silva, M. 2004. Seismic inversion methods and some of their constraints; First Break 22 47–70.

Veeken, P. C. H., and Rauch-Davies, M. 2006. AVO attribute analysis and seismic reservoir characterization; First Break 24 41–52, https://doi.org/10.3997/1365-2397.2006004.

Walls, J., Dvorkin, J., and Carr, M. 2004. Well logs and rock physics in seismic reservoir characterization; Offshore Technol. Conf., https://doi.org/10.4043/16921-MS.

Wang, Y. 2017. Seismic Inversion: Theory and Applications, Wiley Blackwell.

White, R. 2003. Tying well-log synthetic seismograms to seismic data: The key factors; In: SEG Technical Program Expanded Abstracts 2003, Society Exploration Geophysicists, pp. 2449–2452, https://doi.org/10.1190/1.1817885.

Wyllie, M. R. J., Gregory, A. R., & Gardner, L. W. (1956). Elastic wave velocities in heterogenous and porous media. *Geophysics, 21(1)*, 41-70.

Yao, F., and Gan, L. 2000. Application and restriction of seismic inversion; Pet. Explor. Dev. 27 53–56.

Yilmaz, Ö. 2001. Seismic data analysis: Processing, inversion, and interpretation of seismic data, investigations in geophysics; Society of Exploration Geophysicists, https://doi.org/10.1190/1.9781560801580.